



Global surface reflectance products from Landsat: Assessment using coincident MODIS observations

Min Feng ^{a,*}, Joseph O. Sexton ^a, Chengquan Huang ^a, Jeffrey G. Masek ^b, Eric F. Vermote ^c, Feng Gao ^d, Raghuram Narasimhan ^a, Saurabh Channan ^a, Robert E. Wolfe ^c, John R. Townshend ^a

^a Global Land Cover Facility, Department of Geography, University of Maryland, College Park, MD 20742, USA

^b Biospheric Sciences Branch, NASA Goddard Space Flight Center, Greenbelt, MD 20771, USA

^c Laboratory for Terrestrial Physics, NASA Goddard Space Flight Center, Greenbelt, MD 20771, USA

^d Hydrology and Remote Sensing Lab, USDA Agricultural Research Service, Beltsville, MD 20705, USA

ARTICLE INFO

Article history:

Received 13 September 2011

Received in revised form 24 February 2013

Accepted 24 February 2013

Available online 10 April 2013

Keywords:

Landsat
Surface reflectance
Global
MODIS
Quality assessment

ABSTRACT

Global, long-term monitoring of changes in Earth's land surface requires quantitative comparisons of satellite images acquired under widely varying atmospheric conditions. Although physically based estimates of surface reflectance (SR) ultimately provide the most accurate representation of Earth's surface properties, there has never been a globally consistent SR dataset at the spatial resolution (<1 ha) or temporal extent (~40 years) of the Landsat mission. To increase the consistency and robustness of Landsat-based land cover monitoring, we atmospherically corrected the Global Land Survey (GLS) Landsat dataset using the Landsat Ecosystem Disturbance Adaptive Processing System (LEDAPS) implementation of the Second Simulation of the Satellite Signal in the Solar Spectrum (6S) radiative transfer model. The GLS provides synoptic, orthorectified, cloud-free Landsat coverage of Earth's land area in four nominal epochs (1975, 1990, 2000, and 2005). This paper presents the resulting GLS surface reflectance dataset and a global assessment of the 2000- and 2005-epoch data against coincident Moderate Resolution Imaging Spectroradiometer (MODIS) daily SR and Normalized Bidirectional Distribution Function-Adjusted Reflectance (NBAR) measurements. Agreement with respect to MODIS SR and NBAR data is very high, with overall discrepancies (Root-Mean-Squared Deviation (RMSD)) between 1.3 and 2.8 percent reflectance for Landsat-7 Enhanced Thematic Mapper Plus (ETM+) and between 2.2 and 3.5 percent reflectance for Landsat-5 Thematic Mapper (TM). The resulting Landsat surface reflectance dataset and the associated quality metrics for each image are hosted on the Global Land Cover Facility web site for free download (http://www.landcover.org/data/gls_SR). This new repository will provide consistent, calibrated, multi-decadal image data for robust land cover change detection and monitoring across the Earth sciences.

© 2013 Elsevier Inc. All rights reserved.

1. Introduction

Global, long-term monitoring of land-cover change is a central and long-standing goal of the Earth sciences (Goward & Williams, 1997; Huang et al., 2009; Townshend et al., 1991). Consistency and repeatability in this arena require that the basic image-to-image comparisons be based on data represented on the same thematic scale of measurement (Sexton et al., 2013; Song et al., 2001; Stevens, 1946). Although radiance – the rate of energy leaving a surface – is a more basic scale for representing remotely sensed measurements, radiance varies with illumination and viewing geometry, incoming radiation, and atmospheric conditions (Chander et al., 2009). Alternatively, reflectance – the ratio of outgoing to incoming radiance – provides a more robust representation of Earth's surface over varying external conditions (Kaufman & Tanré, 1996; Vermote et al., 1997a).

Surface reflectance (SR) datasets have been produced from data collected by space-borne sensors operating at various spatial and temporal scales, including the Moderate Resolution Imaging Spectroradiometer (MODIS) (Vermote et al., 2002), Advanced Very High Resolution Radiometer (AVHRR) (Kangas et al., 2001), and Advanced Spaceborne Thermal Emission and Reflection Radiometer (ASTER) (Yamaguchi et al., 1998). The Landsat series of sensors have been collecting measurements uniquely scaled for monitoring land cover change since 1972, but there has never been a standard surface reflectance product associated with the Landsat mission (Masek et al., 2006). To increase the comparability of Landsat data over space and time and to data from other sensors, there is a need to retrieve estimates of surface reflectance from this valuable record of Earth's recent history (Vermote et al., 2006).

Estimates of Earth's surface reflectance, SR, are retrieved by adjusting measurements of at-sensor, or “Top of Atmosphere” (TOA), reflectance for atmospheric transmission and scattering. Based on the software architecture of MODIS Adaptive Processing System (MODAPS)

* Corresponding author. Tel.: +86 15001192931.
E-mail address: feng.tank@gmail.com (M. Feng).

(Masuoka et al., 2007), the Landsat Ecosystem Disturbance Adaptive Processing System (LEDAPS) is a codebase for atmospheric correction of Landsat data to enable rapid retrieval of SR from large quantities of Landsat images stored as quantized digital numbers (Masek et al., 2006). It can be applied to any Landsat image for which radiometric gains and biases are available. Using Landsat images assembled through the joint National Aeronautics and Space Administration (NASA) – U.S. Geological Survey (USGS) Global Land Survey (GLS) (Franks et al., 2009; Gutman et al., 2008; Tucker et al., 2004), LEDAPS is being used to create global SR datasets in nominal 1975, 1990, 2000, and 2005 “epochs”, which will serve as the benchmark first global surface reflectance datasets at the Landsat scale. Previously, we developed a Landsat–MODIS Consistency Checking System (LMCCS) for evaluating Landsat SR products using near-simultaneous MODIS observations (Feng et al., 2012). In this paper, we use the LMCCS to assess the quality of the global

Landsat SR datasets developed using GLS 2000 and 2005 as compared with MODIS observations.

Masek et al. (2006) introduced the LEDAPS system for atmospheric correction of Landsat images. Tucker et al. (2004) and Gutman et al. (2008) describe the development and characteristics of the GLS Landsat dataset. After briefly reviewing the adaptation of LEDAPS for retrieving SR across the 2000 and 2005 GLS epochs, this paper presents the resulting Landsat-based global surface reflectance dataset through an assessment of its agreement with coincident surface reflectance retrievals from MODIS, with respect to known radiometric calibration uncertainties of the two instruments. Although this should be considered a relative assessment, the high quality of the MODIS data, as well as their global coverage, provides the best available reference for global comparison (Vermote & Kotchenova, 2008a; Vermote et al., 2002; Wang et al., 2009). For more absolute (i.e., ground-based) validations

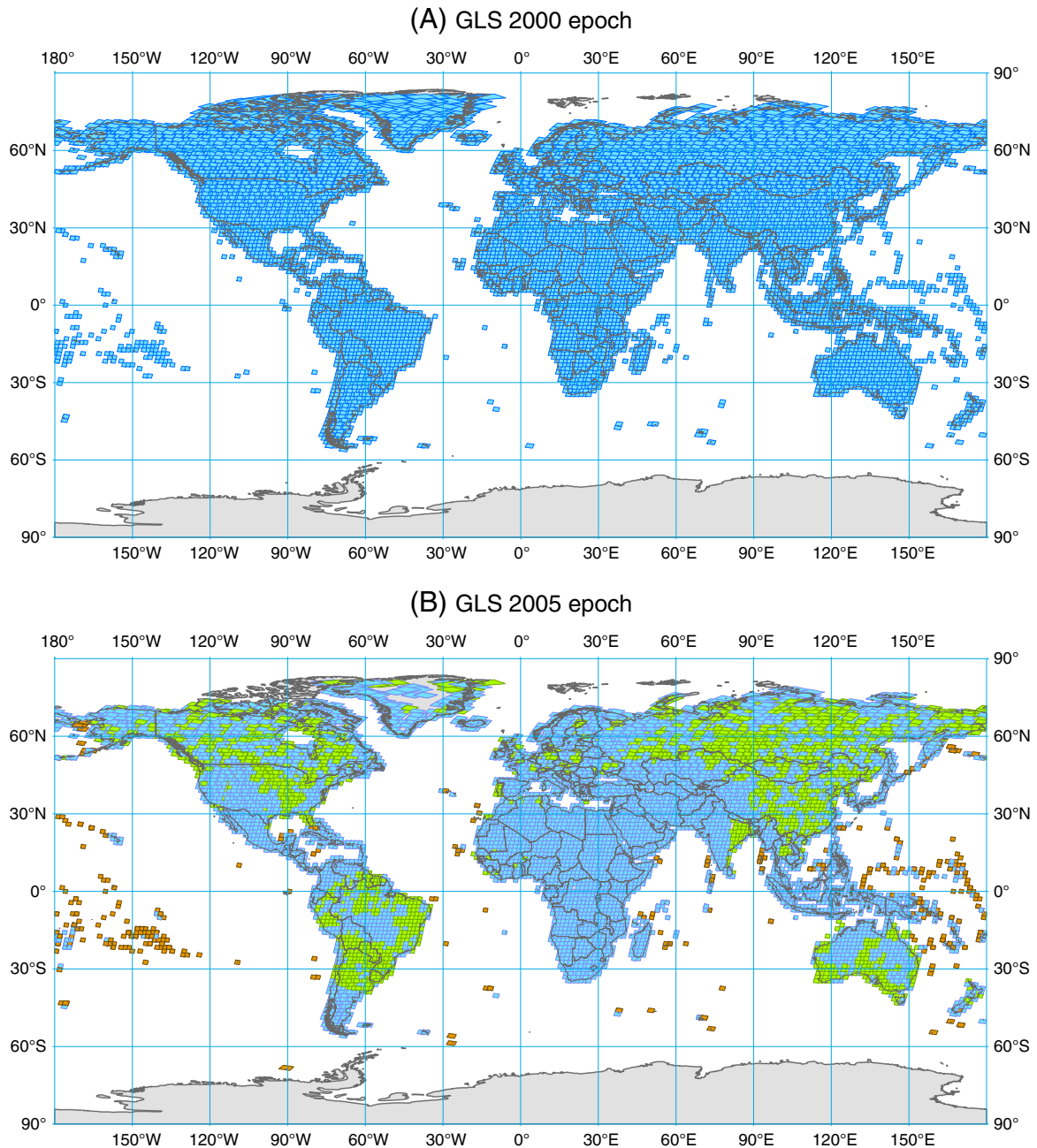


Fig. 1. Global coverage of GLS 2000 (A) and 2005 (B) epochs. TM images are represented in green, ETM+ in blue, and EO-1 ALI images (which are not addressed in this paper) in brown.

Table 1

The six 30-m solar-reflective bands of Landsat TM and ETM+ and their most similar counterparts from MODIS.

Band	MODIS band	MODIS bandwidth (nm)	TM band	TM bandwidth (nm)	ETM+ band	ETM+ bandwidth (nm)
B	3	459–479	1	450–520	1	450–520
G	4	545–565	2	520–600	2	520–600
R	1	620–670	3	630–690	3	630–690
NIR	2	841–876	4	760–900	4	770–900
SWIR1	6	1628–1652	5	1550–1750	5	1550–1750
SWIR2	7	2105–2155	7	2080–2350	7	2090–2350

of Landsat and MODIS SR based on smaller samples of near-surface measurements, refer to Ju et al. (2012), Masek et al. (2006), and Vermote et al. (2002).

2. Data and methods

2.1. The Global Land Survey Landsat dataset

The GLS is a partnership between USGS and NASA, in support of the U.S. Climate Change Science Program and the NASA Land-cover and Land-use Change (LCLUC) Program. Building on the existing GeoCover dataset developed for the 1970s, 1990, and 2000 (Tucker et al., 2004), the GLS was selected to provide wall-to-wall, orthorectified, cloud-free Landsat coverage of Earth's land area at 30-meter resolution in nominal "epochs" of 1975, 1990, 2000, and 2005 (Franks et al., 2009; Gutman et al., 2008). A follow-up GLS dataset is being developed for the 2010 epoch, which is nearing completion as of the writing of this paper. The GLS is intended to provide one clear-view image acquired during the peak growing season of each epoch for each World Reference System (WRS) scene. In many cases, however, images had to be selected with a date outside this range, mostly due to lack of cloud-free images during the growing season (Franks et al., 2009; Gutman et al., 2008). Because images have been selected from somewhat different dates,

there are variations in phenology which accounts for the patchiness of image mosaics in many locations (Kim et al., 2011; Townshend et al., 2012).

The GLS 1975 is composed of 7337 Landsat-1 and Landsat-2 Multi-Spectral Scanner (MSS) images acquired between 1972 and 1984, the GLS 1990 by 7375 Landsat-5 Thematic Mapper (TM) images from 1984 to 1997, and the GLS 2000 (Fig. 1A) by 8756 Landsat-7 Enhanced Thematic Mapper Plus (ETM+) images from 1999 to 2002. Due to the failure of the Landsat-7 ETM+ Scan Line Corrector (SLC) in 2003, the GLS 2005 (Fig. 1B) is composed of a combination of 7284 gap-filled Landsat-7 images and 2424 Landsat-5 TM images from U.S. and international ground stations acquired between 2003 and 2008. The GLS 2005 also includes a Landsat image mosaic for Antarctica (<http://lima.usgs.gov>) and supplemental images from ASTER and Earth Observing-1 Advanced Land Imager (EO-1 ALI) to increase coverage over small islands. This study is based solely on the GLS 2000 and 2005 Landsat images; however, accuracies reported here should be representative of SR products derived using the GLS 1990, GLS 2010, and other Landsat-5 and -7 images that have proper radiometric calibration parameters.

2.2. Retrieval of SR by atmospheric correction

The LEDAPS surface reflectance algorithm (Masek et al., 2006) is based on the MODAPS approach for retrieving SR estimates from MODIS images. Assuming that Earth is an infinite, Lambertian surface and that gaseous absorption and particle scattering in the atmosphere can be decoupled, LEDAPS uses the 6S radiative transfer model (Vermote et al., 1997b) to compute transmission, intrinsic reflectance, and spherical albedo for relevant atmospheric constituents—including gases, ozone, water vapor, and aerosols. LEDAPS then calculates SR by compensating for these atmospheric scattering and absorption effects to atmospherically correct TOA reflectance to SR.

Atmospheric variables were gathered from various data sources. Ozone concentration was derived from the Total Ozone Mapping Spectrometer (TOMS) aboard the Nimbus-7, Meteor-3, and Earth Probe

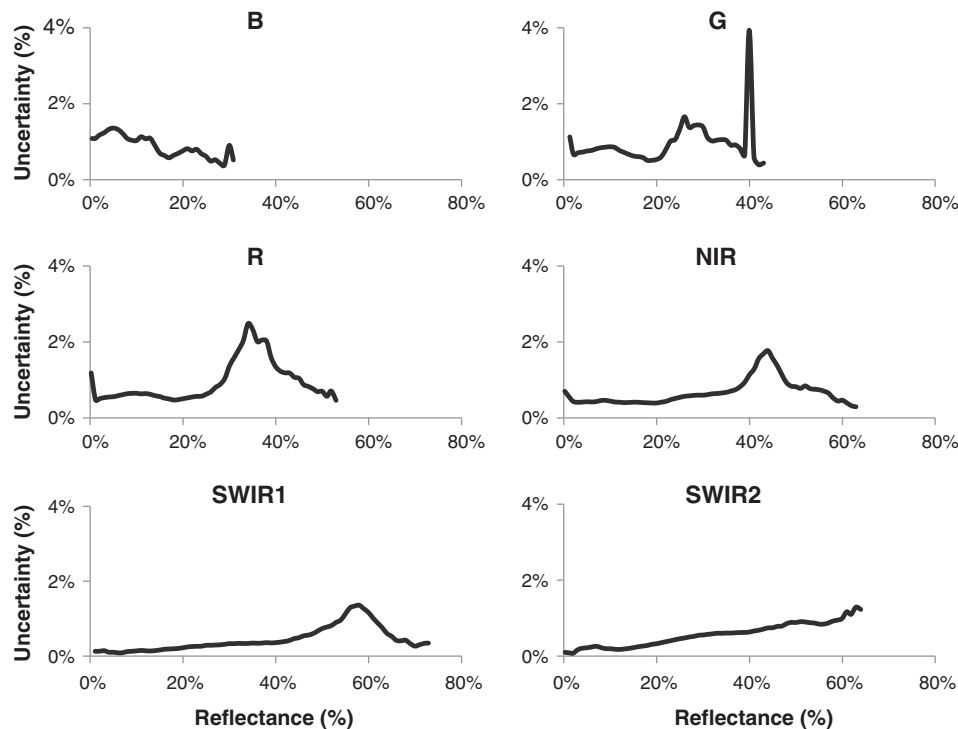


Fig. 2. Measurement uncertainties (1σ) of MODIS SR data in the R, G, R, NIR, SWIR1, and SWIR2 bands (calculated following the methods of Vermote and Kotchenova (2008a)).

platforms and from NOAA's Television Infrared Observation Satellite Program (TIROS) Operational Vertical Sounder (TOVS) when TOMS data were not available. Column water vapor was taken from NOAA National Centers for Environmental Prediction (NCEP) re-analysis data (available at <http://dss.ucar.edu/datasets/ds090.0/>). A digital topography dataset at 0.05 deg (derived from the 1 km GTopo30) and NCEP surface pressure data were used to adjust Rayleigh scattering to local conditions. Aerosol optical thickness (AOT) was derived empirically from each Landsat image using the dark dense vegetation method (Kaufman & Tanré, 1996), or using relationships between red and blue bands and the SWIR band, as demonstrated by Vermote and Saleous (2006). A default AOT value of 0.06 at 550 nm was used when a valid value could not be retrieved using the dark dense vegetation method or derived through spatial interpolation.

2.3. Quality assessment

2.3.1. Landsat–MODIS comparison

Comparisons were performed between MODIS daily SR (MOD09GA) (Vermote & Kotchenova, 2008b; Vermote et al., 2002) and 16-day Nadir Bidirectional Reflectance Distribution Function-Adjusted Reflectance (NBAR) data products (MCD43A4) (Schaaf et al., 2002) at 500-m resolution. Reflectance estimates were collected from samples of Landsat and MODIS pixels using an algorithm designed by Feng et al. (2012) to acquire, overlay, extract, and compare coincident satellite measurements. Comparisons were then made over the pooled global sample for an overall global quality assessment and also mapped across Landsat Worldwide Reference System-2 (WRS-2) scenes to show spatial patterns of data quality, as recommended by Schaaf et al. (2002). Following Masek et al.'s (2006) conclusion of the comparability of Landsat and MODIS bands, each of the six Landsat TM and ETM+ solar-reflective spectral bands were matched with its most similar MODIS band (Table 1). Landsat-7 and MODIS Terra follow the same orbit, and their equatorial crossing times differ by only about 30 min (i.e., 10:00–10:15 AM for Landsat-7 vs. 10:30 for Terra) (Landsat 7 Science Data Users Handbook, 2009). However, orbits of Landsat-5 and Terra MODIS differ greatly, potentially leading to spurious disagreement of SR retrievals due to BRDF effects (Roy et al., 2008). We therefore compared the TM SR with the MODIS NBAR product, which is computed for the mean solar zenith angle of each 16-day period (Schaaf et al., 2002). Although temporal resolution differs between MODIS NBAR and Landsat SR, preliminary evaluations confirmed that this effect was less than that imposed by changing BRDF (Roy et al., 2008). ETM+ images were thus paired with coincident MODIS daily SR images, and TM images were paired with the closest MODIS NBAR images in time.

A systematic joint sample of Landsat and coincident MODIS SR (or NBAR) pixel values was extracted from within the extent of each Landsat image. To mitigate resolution differences between the two sensors, Landsat values were aggregated to MODIS resolution by averaging Landsat values within the extent of each sampled MODIS pixel. The sample coordinates were selected by picking one out of nine MODIS pixels in both horizontal and vertical directions within the overlapping region of the two images (Feng et al., 2012). The sample was then filtered to exclude heterogeneous pixels, pixels contaminated by clouds and/or their shadows, and pixels whose viewing zenith angle was different between Landsat and MODIS. In the MODIS data, cloud and shadow were identified using the MOD09 internal masks from the MODIS Quality Assessment (QA) band (Vermote & Kotchenova, 2008b). Because cloud cover was minimized in selecting the GLS images (Tucker et al., 2004), we did not check for cloud cover in the Landsat images. Some MODIS SR images were affected by poorly calibrated detectors early in the mission of MODIS Terra (Xiong et al., 2007), and the erroneous values can lead to unexpected disagreement for the Landsat SR quality assessment; we visually checked the MODIS images acquired in 2000 to identify images with erroneous pixels and then filtered the samples collected

from these images. Systematic quality issues identified by our analysis were resolved to avoid impact to the final dataset.

2.3.2. Agreement measures

Consistency metrics were based on those recommended by Willmott (1982) and supporting linear regression parameters for each spectral band. Agreement was quantified by Mean Bias Error (MBE) and Root-Mean-Squared Difference (RMSD):

$$MBE = \sum_{i=1}^n \frac{L_i - M_i}{n} \quad (1)$$

$$RMSD = \sqrt{\frac{\sum_{i=1}^n (L_i - M_i)^2}{n}} \quad (2)$$

where L_i and M_i are SR values derived from Landsat and MODIS, respectively, at a sample location i and n is the count of joint observations in the sample. After modeling the relationship between L and M , the (squared) difference between L and M is disaggregated into systematic error (MSE_S) and unsystematic error (MSE_U) based on a modeled linear relationship:

$$MSE_S = \sum_{i=1}^n \frac{(\hat{L}_i - M_i)^2}{n} \quad (3)$$

$$MSE_U = \sum_{i=1}^n \frac{(L_i - \hat{L}_i)^2}{n} \quad (4)$$

where \hat{L}_i is the MODIS equivalent of a Landsat-derived SR value predicted by the modeled relationship ($Y = \alpha + \beta X$) between L and M . Considering that both MODIS and Landsat SR values have uncertainties, Reduced Major Axis (RMA) regression (Berterretche et al., 2005; Cohen et al., 2003; Sokal & Rohlf, 1994) was used instead of the standard, ordinary least squares (OLS) regression to fit the parameters α (intercept), β (slope), and R^2 :

$$\beta = \pm(S_{ML}) \frac{\frac{S_L}{S_M} \pm \left(\frac{1}{n-1} \sum_{i=1}^n (L_i - \bar{L})(M_i - \bar{M}) \right)}{\sqrt{\frac{\sum_{i=1}^n (L_i - \bar{L})^2}{n-1}}} \quad (5)$$

$$\alpha = \bar{L} - \beta \bar{M} \quad (6)$$

$$R^2 = \frac{S_{ML}^2}{S_M S_L} = \frac{(\sum_{i=1}^n (L_i - \bar{L})(M_i - \bar{M}))^2}{(\sum_{i=1}^n (M_i - \bar{M})^2)(\sum_{i=1}^n (L_i - \bar{L})^2)} \quad (7)$$

where \bar{M} , S_M , \bar{L} , and S_L are mean and sample variance of M and L respectively, and S_{ML} is covariance of M and L (Sokal & Rohlf, 1994).

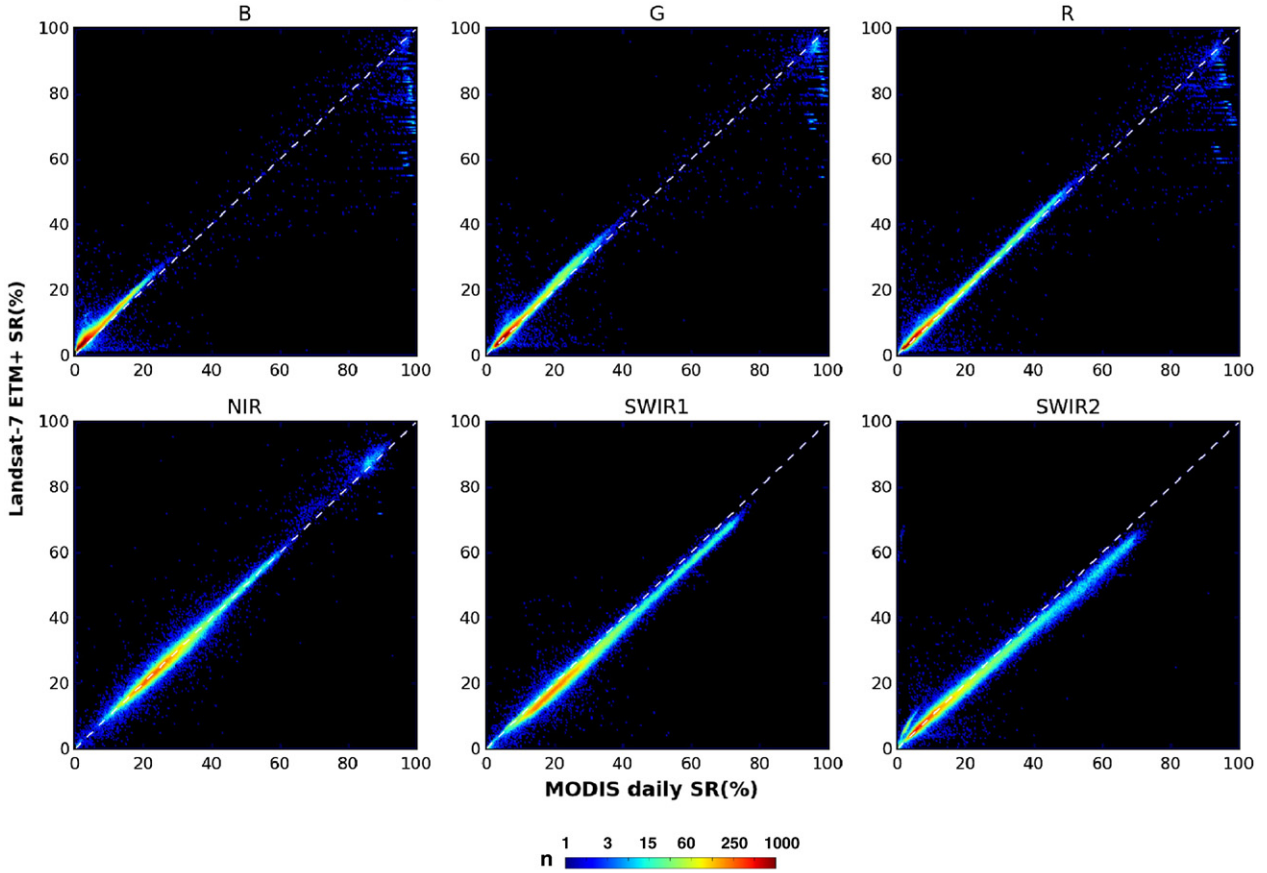
Systematic error measures the difference between the trend of Landsat- and MODIS-based SR, and the variation surrounding that trend is quantified by the unsystematic error. MSE_S and MSE_U sum to Mean-Squared Difference (MSD), and therefore:

$$RMSD = \sqrt{MSE_S + MSE_U} \quad (8)$$

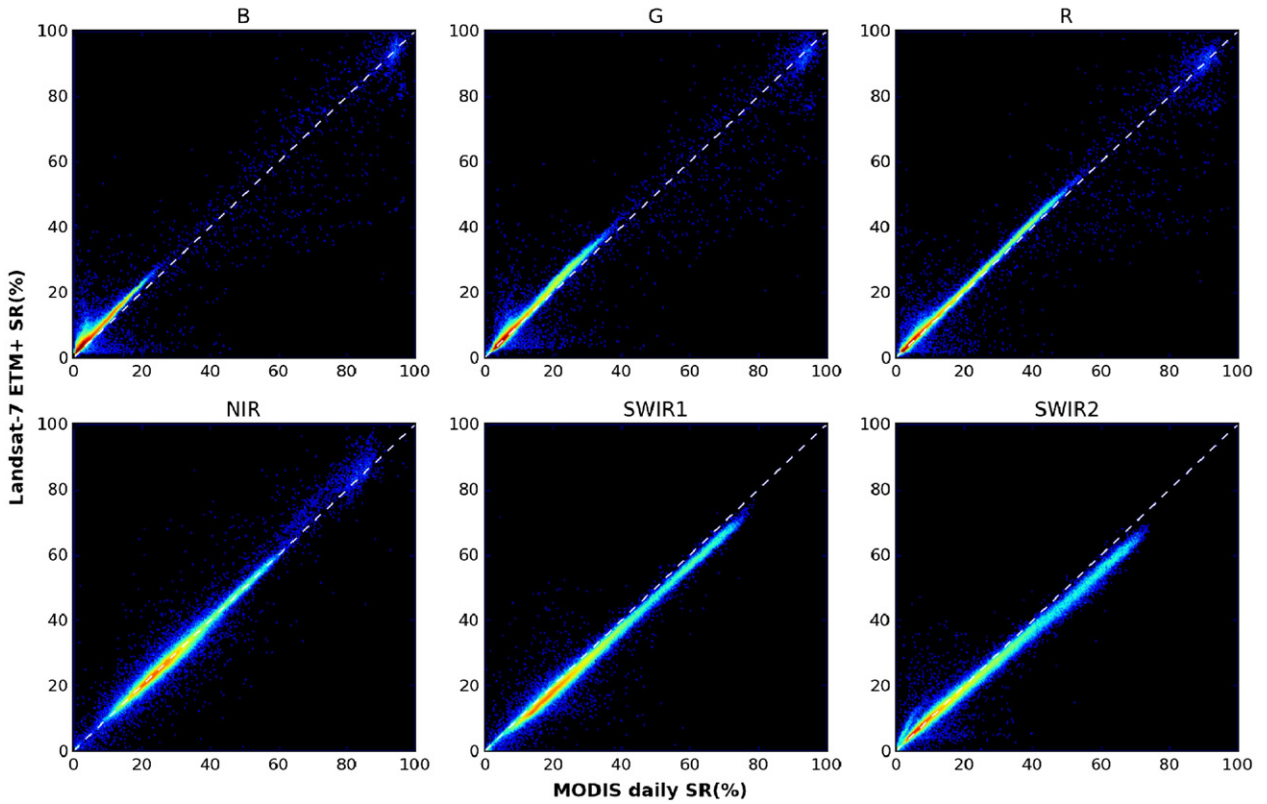
To maintain consistent units, we report the square roots of MSE_S and MSE_U , i.e., $RMSD_S$ and $RMSD_U$, in units of percent reflectance.

Part of the disagreement between Landsat and MODIS SR values is likely due to measurement errors of the two satellites. Absolute calibration uncertainties (1σ) of the reflective bands are 7% and 5% for Landsat 5 TM and Landsat 7 ETM+, respectively (Markham & Helder, 2012). Following the methods of Vermote and Kotchenova (2008a), we calculated the uncertainties for the 6 reflective bands in MODIS data (Fig. 2). Since these two types of uncertainties are

(A) GLS 2000 ETM+ vs. MODIS daily SR



(B) GLS 2005 ETM+ vs. MODIS daily SR



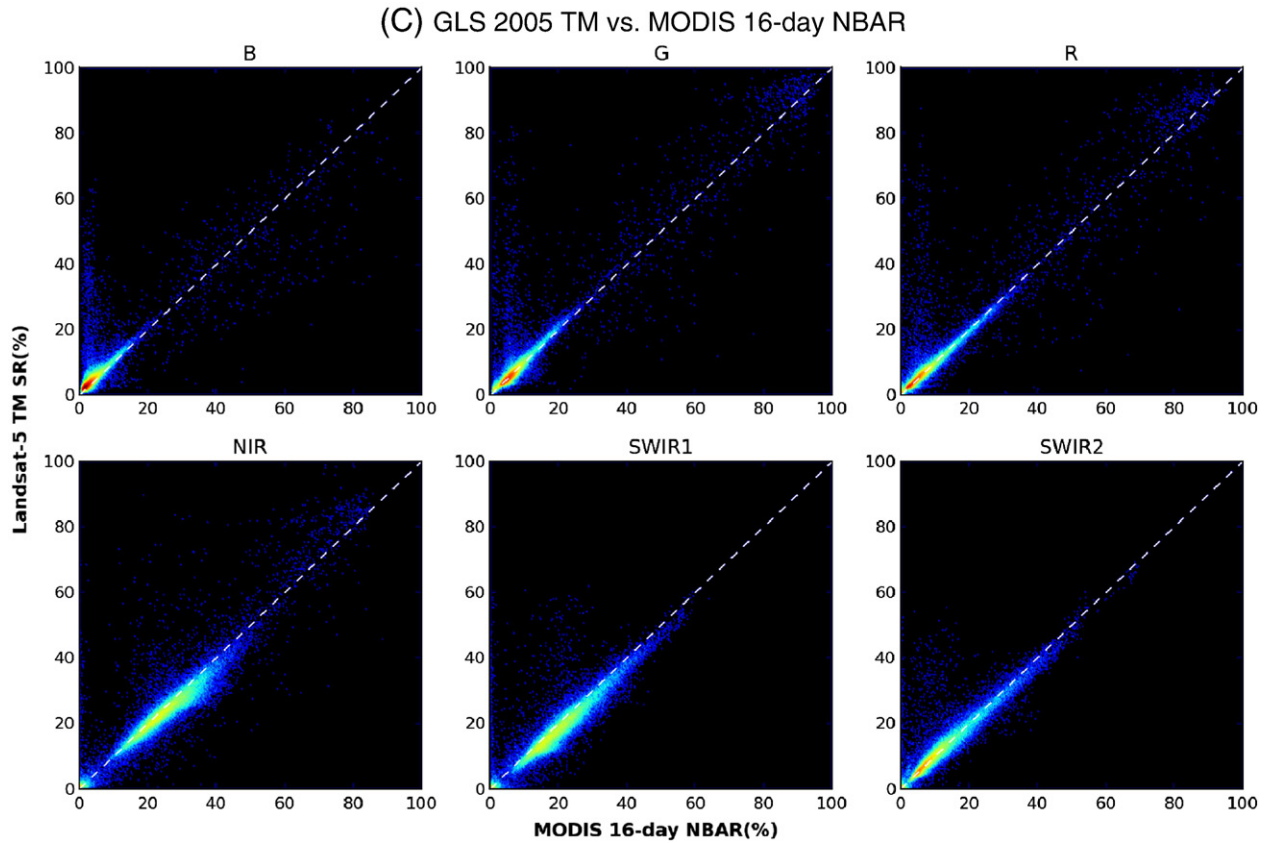


Fig. 3. Density plots computed over the samples pooled across the global Landsat images for the six bands (i.e., B, G, R, NIR, SWIR1, and SWIR2) of GLS 2000 and 2005. Figures (A) and (B) show the scatter plots for GLS 2000 and GLS 2005 respectively, with MODIS daily SR as x-axis and Landsat-7 ETM+ SR as y-axis. Figure (C) shows the scatter plots for GLS 2005 with MODIS 16-day NBAR as x-axis and Landsat-5 TM SR as y-axis.

independent, disagreement between Landsat and MODIS data (1σ) that may arise from such uncertainties ($RMSD_{INST}$) can be calculated as:

$$RMSD_{INST} = \sqrt{\frac{\sum_{i=1}^n (ERR_M)^2 + (ERR_L)^2}{n}} \quad (9)$$

where ERR_M is the uncertainty (1σ) of MODIS data as described by Fig. 2. ERR_L is the absolute calibration uncertainty of Landsat data, which is 7% of TM measurements and 5% of ETM+ measurements (Markham & Helder, 2012).

MBE and $RMSD$ share the scale of the input data, the range of which can lead to difficulties in comparing accuracies of bright and dark targets. In order to evaluate and compare $RMSD$ calculated from different

Table 2

Summary of global comparison between SR derived from GLS 2000 & 2005 Landsat (Landsat-5 TM and Landsat-7 ETM+) and coincident MODIS SR (daily SR and 16-day NBAR compared with ETM+ and TM respectively). The metrics reported are global averages among available GLS Landsat scenes. Values are represented as percent reflectance (%) for intercept, $RMSD$, $RMSD_S$, $RMSD_U$, and MBE .

Epoch	Sensor	Band	n	Slope	Intercept	R ²	RMSD	RMSD _S	RMSD _U	MBE	RMSD _R
2000	ETM+	B	214,893	1.057	2.493	0.785	2.188	1.996	0.662	0.96	1.557
		G	214,843	1.015	1.105	0.847	1.425	1.132	0.696	0.242	1.291
		R	214,779	1.016	1.255	0.876	1.386	1.033	0.753	0.140	1.460
		NIR	214,923	1.024	-0.993	0.896	1.728	0.971	1.297	-0.34	1.153
		SWIR1	214,941	0.980	-1.742	0.901	2.672	2.314	1.116	-2.174	2.603
		SWIR2	213,850	0.972	-0.011	0.886	1.856	1.393	0.971	-0.772	2.412
2005	ETM+	B	202,238	1.035	1.295	0.777	2.282	2.016	0.838	1.320	1.732
		G	202,839	0.974	0.345	0.831	1.706	1.320	0.895	0.378	1.564
		R	202,663	1.075	0.057	0.858	1.593	1.154	0.935	0.348	1.736
		NIR	203,113	1.019	-0.845	0.891	1.956	1.085	1.493	-0.279	1.252
		SWIR1	203,125	0.964	-1.241	0.891	2.770	2.342	1.240	-2.092	2.724
		SWIR2	203,097	0.963	0.205	0.868	1.987	1.467	1.097	-0.702	2.618
	TM	B	94,915	1.197	0.283	0.562	2.547	1.906	1.544	0.974	1.718
		G	95,866	1.044	-0.135	0.697	2.280	1.552	1.558	0.409	1.884
		R	95,783	1.052	0.027	0.760	2.261	1.483	1.605	0.428	2.126
		NIR	95,562	0.991	-1.422	0.810	3.434	2.305	2.296	-1.130	1.925
		SWIR1	95,906	0.990	-2.638	0.789	3.404	2.461	2.089	-1.636	2.800
		SWIR2	95,905	1.066	-0.521	0.802	2.261	1.406	1.655	0.171	2.679

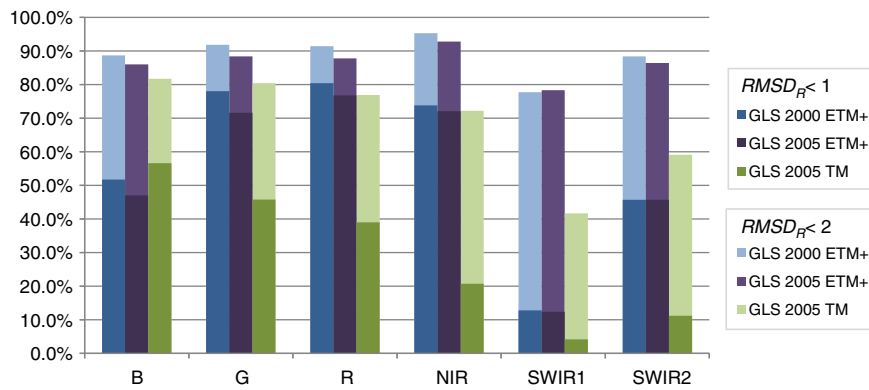


Fig. 4. Percentage of Landsat images with Landsat–MODIS differences within 1σ ($RMSD_R < 1$) and 2σ ($RMSD_R < 2$) of the combined instrument uncertainties of the two satellites.

images, we report $RMSD_R$, a ratio between $RMSD$ of each image and its $RMSD_{INST}$:

$$RMSD_R = RMSD / RMSD_{INST} \quad (10)$$

Spatial distributions of the $RMSD_R$ for Landsat SR images are illustrated in global maps, showing the geographic patterns of the Landsat SR image quality as measured by agreement with MODIS data. An $RMSD_R$ value of less than 2 indicates that the observed disagreement between Landsat and MODIS SR values is within 2σ of the measurement uncertainties of the two satellites.

2.4. Processing and distribution

LEDAPS was used to retrieve surface reflectance estimates from the Landsat GLS 2000 and 2005 digital number (DN) data. The C and FORTRAN codebase and the associated libraries were ported from a 32- to a 64-bit Linux environment. The Landsat–MODIS comparison was developed in JAVA (Feng et al., 2012). The ancillary, input, and output data were stored on Oracle's StorageTek 2540. Leveraging Network File System (NFS) and PERL scripts were developed in-house to automate the process, and the jobs were batched and distributed to 12 processing nodes (Oracle SunFire 4150). Using this system, 18,462 Landsat images were converted to SR in about 4 days. The output data were in Universal Transverse Mercator (UTM) projection with the World Geodetic System (WGS)-84 datum, consistent with the input Landsat DN data, and stored internally in Hierarchical Data Format (HDF 4) file format; however, to keep the format consistent with the

GLCF archive, the data were then converted to GeoTIFF, compressed, and made available online (http://www.landcover.org/data/gls_SR). Because of differences in calibration, the distributed data do not include ALL.

3. Results

3.1. Global assessment against MODIS SR products

Correlation between SR retrieved from Landsat ETM + and the MODIS daily SR product was strong in every band and for both 2000 and 2005 epochs (Fig. 3). The range of measured reflectance increased in proportion to wavelength, with the visible bands recording less variation in both MODIS and Landsat estimates than IR bands. The distribution of each band was bimodal, with clouds and snow in both images forming a diffuse minor mode at high values in both MODIS and Landsat SR. The dominant mode of each band's distribution comprised data from mostly clear pixels from both sensors, and the structure of each band's correlation changed little between 2000 and 2005. The magnitudes of the secondary modes were proportional to wavelength, with the visible bands more affected by residual clouds and snow than the infrared bands.

Deviations between Landsat-7 ETM + and MODIS SR, as measured by $RMSD$, ranged from 1.3 to 2.8 percentage points of reflectance (Table 2), or about 20% of the dynamic range of reflectance over vegetated surfaces. Most of this uncertainty was accounted for by systematic differences between the measurements from the two sensors; $RMSD_S > RMSD_U$ in all bands except NIR. Bias (MBE) was consistently close to zero, ranging

Table 3
Global summary of comparison between GLS 2000 and 2005 Landsat (Landsat-7 ETM+) derived SR and coincident MODIS daily SR estimates after removing samples from snow-covered images. The metrics reported are global averages among available GLS Landsat scenes. Values are represented as percent reflectance (%) for *intercept*, $RMSD$, $RMSD_S$, $RMSD_U$, and MBE .

Epoch	Sensor	Band	n	Slope	Intercept	R ²	RMSD	RMSD _S	RMSD _U	MBE	RMSD _R
2000	ETM +	B	208,841	1.079	1.124	0.790	1.781	1.613	0.595	1.319	1.442
		G	208,837	1.029	0.157	0.854	1.174	0.915	0.614	0.378	1.224
		R	208,843	1.034	0.107	0.883	1.078	0.754	0.675	0.329	1.369
		NIR	208,825	1.025	-1.076	0.902	1.610	0.875	1.238	-0.412	1.129
		SWIR1	208,843	0.981	-1.821	0.904	2.704	2.364	1.105	-2.244	2.588
		SWIR2	207,757	0.962	-0.072	0.891	1.807	1.347	0.960	-0.882	2.234
2005	ETM +	B	197,510	1.041	1.183	0.774	2.066	1.842	0.737	1.412	1.665
		G	197,523	0.975	0.393	0.831	1.484	1.155	0.772	0.450	1.503
		R	197,524	1.082	0.009	0.86	1.357	0.972	0.817	0.412	1.665
		NIR	197,555	1.016	-0.729	0.892	1.836	1.002	1.419	-0.352	1.228
		SWIR1	197,560	0.965	-1.301	0.893	2.792	2.386	1.222	-2.157	2.687
		SWIR2	197,537	0.954	0.161	0.872	1.948	1.439	1.077	-0.799	2.477

within -2.2 – 1.4 percentage points (Table 2). Correlations at the global scale were strongly linear, with R^2 higher than 0.8 for all bands except B. The sample sizes were on the order of 10^5 observations, and p -values were all <0.05 . Correspondingly, intercepts were near zero and slopes were close to 1:1, although outliers – including saturation of the Landsat sensor over snowy areas (see Section 3.2) – negatively impacted regression parameters in the visible bands.

Correspondences between Landsat-5 TM-based SR and the most coincident 16-day MODIS NBAR values were similar to those between ETM+ and MODIS daily SR. However, the spread of the data was wider (Fig. 3C) and deviations ($RMSD$) ranged from 2.2 to 3.5 percentage points (Table 2), presumably due to surface and atmospheric variation over the 16-day compositing window of MODIS as well as the lower radiometric precision of the TM sensor compared to ETM+ (Chander et al., 2009). The effect of differences in cloud cover between Landsat TM acquisition and the composited MODIS NBAR product was less than that observed between Landsat ETM+ and coincident MODIS SR, as the secondary mode was nearly absent from the joint distribution in all bands.

Significant portions of the observed differences between Landsat and MODIS SR values were likely due to instrument errors of the two systems. Over 70% of the ETM+ images had Landsat–MODIS differences within 1σ of the combined uncertainties of the two systems in the green, red, and NIR bands, i.e., $RMSD_R < 1$, and for the blue and SWIR2 bands the percentages were near 50% (Fig. 4). Except for the SWIR1 band, about 90% of the ETM+ images had Landsat–MODIS differences within 2σ of the combined uncertainties of the two systems. Assuming the normal distribution for uncertainty in both Landsat and MODIS data (i.e. about 68% and 95% of the populations distributed within 1σ and 2σ , respectively), only a small percentage of the ETM+ images had Landsat–MODIS differences exceeding the measurement uncertainties of the two systems for all 6 reflective bands except SWIR1—although those percentages could be higher for the blue and SWIR2 bands. Most of the ETM+ images with Landsat–MODIS differences $> 2\sigma$ (i.e., $RMSD_R > 2$) were located in areas prone to frequent cloud cover (e.g., the tropics) or in high latitude regions mostly covered by snow/ice. The large differences associated with cloudy images were likely the result of cloud movement during the 30 min between Landsat 7 and MODIS overpasses, while saturated Landsat detectors were the likely cause for those associated with images covered mostly by snow/ice (see more discussions in Section 3.2).

Wavelength differences between Landsat and MODIS bands (Table 1) were another likely source of the observed SR differences. In particular, the much narrower bandwidths of the two MODIS SWIR bands made it possible to avoid the spectral ranges with lower atmospheric transmittance that were covered by the Landsat SWIR bands (Lord, 1992). As a result, most Landsat SR values were lower, though only slightly, than the MODIS values in those two bands (Fig. 3), and the SWIR1 band had higher $RMSD_S$ values than any of the other 5 bands (Tables 2 and 3). Given that the MODIS SR values had extremely low uncertainties in the SWIR1 band (Fig. 2), the systematic differences between Landsat and MODIS SR values due to bandwidth differences seemed to be high enough to greatly reduce the percentage of ETM+ images that had $RMSD_R < 1$ (and to a lesser degree for $RMSD_R < 2$) as compared with the other 5 spectral bands (Fig. 4).

In general, the percentages of TM images that had $RMSD_R < 1$ and $RMSD_R < 2$ were lower than those of ETM+ images (Fig. 4). While this is no surprise given that the MODIS NBAR were derived using 16-days of observations and therefore more factors could contribute to the TM–NBAR difference than to the difference between observations obtained within 30 min of each other. Cloud and snow/ice were again the most likely reason for images having $RMSD_R > 3$, because such images were mostly located in high latitude and cloud-prone tropical regions (Fig. 5).

3.2. Further inspection of problematic images

The overall tight correspondence between Landsat and MODIS SR allowed isolated discrepancies to be found between some ETM+ images and their matching MODIS SR images relatively easily (Feng et al., 2012). Further investigation revealed that the disagreements were caused by quality issues with either the Landsat or MODIS input datasets or by inconsistencies in the image metadata. First, although the GLS Landsat data were selected to minimize cloud cover, remnant clouds that may have moved during the ~ 30 -minute overpass difference between Landsat-7 and MODIS Terra magnified error estimates in persistently cloudy regions such as tropical forests. Error estimates for these regions should therefore be considered as upper bounds, with true, cloud-free correspondence better than reported. Second, the inspection uncovered a previously unknown discrepancy in the radiometric gains listed in the metadata of 98 Landsat-7 ETM+ images of the 2000 and 2005 epochs (Appendix 1) for all bands. Although the linear relationship between Landsat and simultaneously acquired MODIS SR was strong ($R^2 > 0.98$), the slope of the relationship in affected images was near 0.7. The input images' metadata revealed that the discrepancies were caused by errors in the ETM+ High/Low (H/L) gains used for rescaling DN values to radiance (Chander et al., 2009). An example ETM+ image acquired on April 12, 2001 over Morocco (WRS-2 path 200/row 37) shows these biases in every band except the NIR band (Fig. 6A). Replacing the gains listed in the image metadata with values recalculated from the LMIN/LMAX values in the metadata provided the correct rescaling parameters, resulting in greatly improved consistency between ETM+ and MODIS surface reflectance (Fig. 6B).

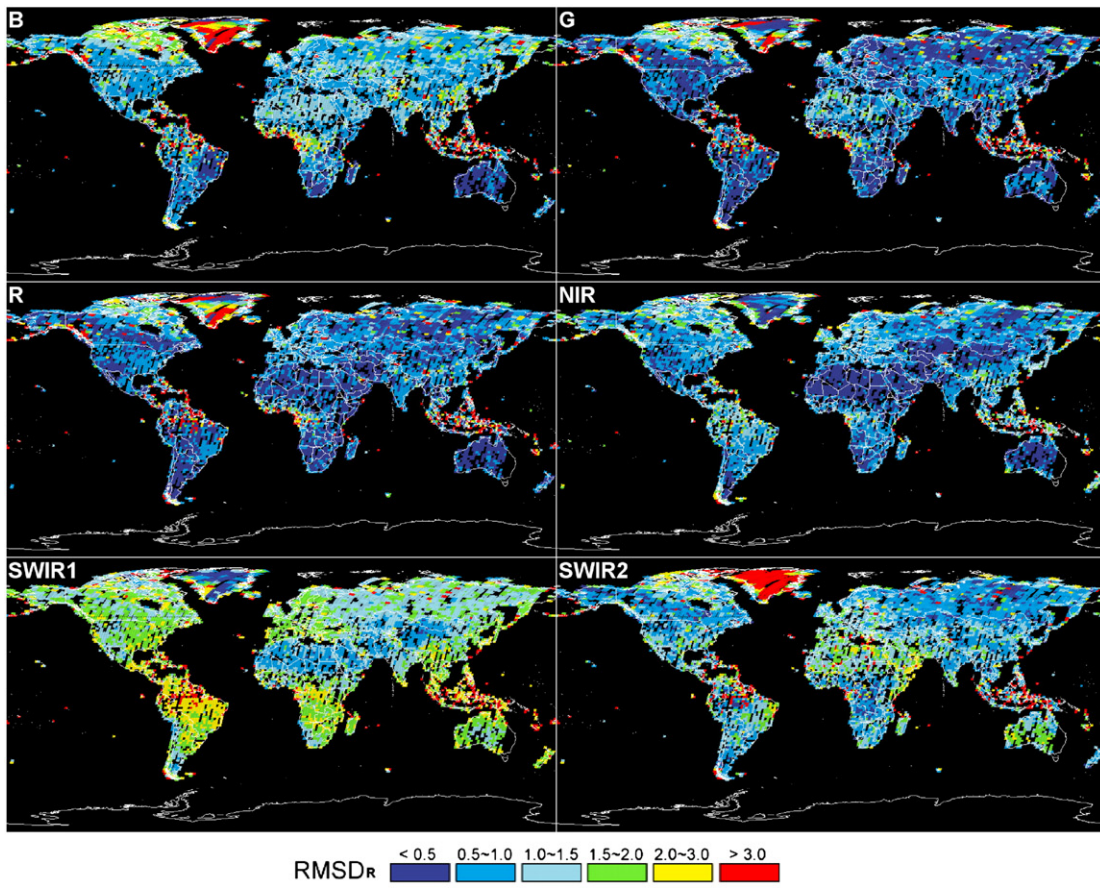
Third, saturation of the 8-bit Landsat sensor by snow and other extremely bright surface types also led to poor correspondence between Landsat- and the (12-bit) MODIS-derived SR values in some images. In such cases, relationships between ETM+ and MODIS values were very weak ($R^2 < 0.1$) in the visible and near-infrared bands. The R^2 values remained relatively high for the SWIR1 and SWIR 2 bands because the reflectance values of snow/ice are lower in these bands (Fig. 7). The contrast of the R^2 values between the SWIR bands and the other 4 bands allowed us to identify Landsat images that had significant saturation problems due to substantial snow cover—234 images in GLS 2000 and 220 images in GLS 2005 were identified thus, checked visually, and removed (Appendix 2).

To evaluate the impact of Landsat saturation on the global quality assessment, we recalculated the metrics after removing images with the issue for both GLS 2000 and 2005 epochs (Table 3). The improvements were quite significant in the visible bands, which were more prone to the saturation problem than the three infrared bands (Fig. 3). The ETM+ images that had saturation problems as identified using the above method comprised about 2.8% of the sample for the 2000 epoch and 2.5% for the 2005 epoch. Removing the affected data reduced $RMSD$ by 10%–23% for the three visible bands, and reduced the regression intercept by $>50\%$ for the blue band and to near 0 for the green and red bands, although the slope increased slightly. Because the three infrared bands were less affected by the saturation problem, there was little change to the various metrics after removing the potentially saturated samples.

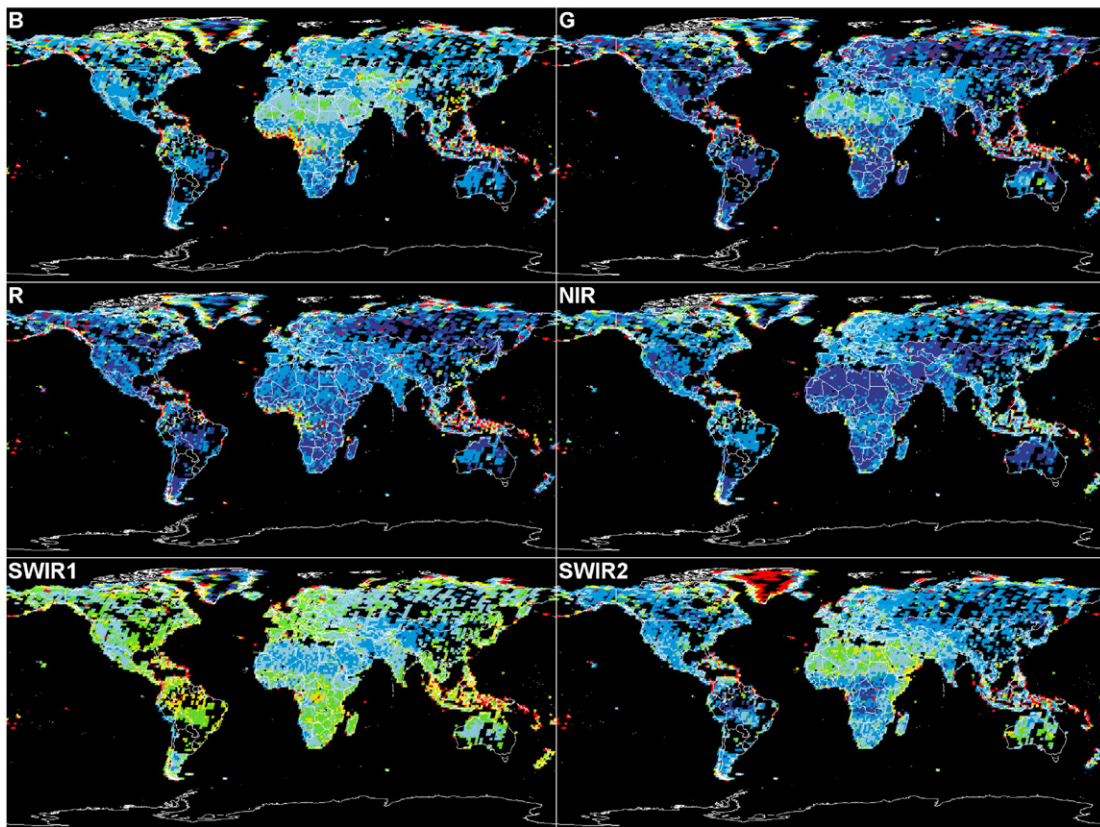
4. Discussion

4.1. The value of surface reflectance for monitoring global change

Among the most fundamental remotely sensed measurements of Earth's land surface, surface reflectance provides a primary, physically-based input for retrieving many higher-level terrestrial attributes such as vegetation indices, albedo, and land cover (Fang et al., 2007; Huete et al., 2002; Myneni et al., 1997; Townshend et al., 2012). Independent of sensor differences, retrieval of surface reflectance provides a more appropriate basis upon which to estimate these surface properties



(A)



(B)

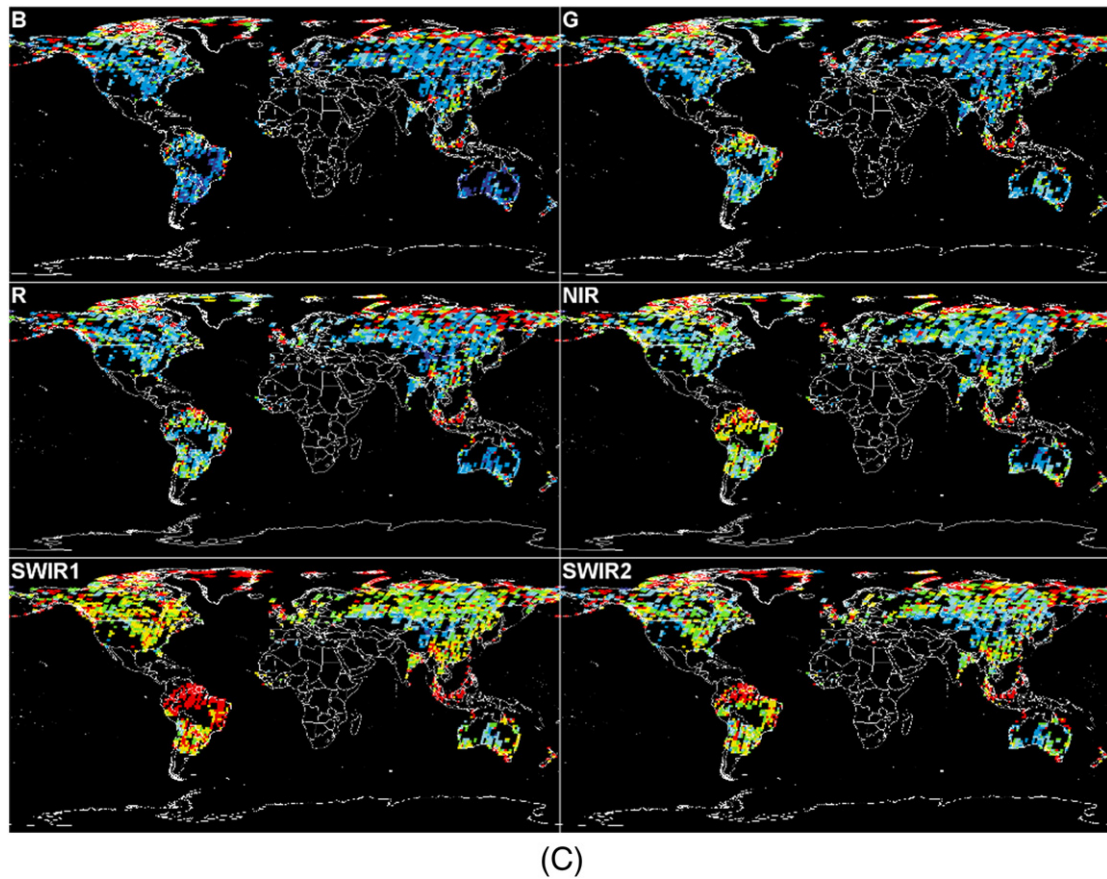


Fig. 5. Global spatial distribution of $RMSD_R$ of ETM + SR images from GLS 2000 (A) GLS 2005 (B) and from TM SR images from GLS 2005 (C). Images with $RMSD_R$ less than 0.5, 1.0, 1.5, 2.0, 3.0, and higher than 3.0 are shown in dark blue, blue, light blue, green, yellow, and red, respectively.

than do arbitrarily scaled DN or uncorrected radiance and TOA reflectance (Vermote et al., 2002). Use of surface reflectance allows researchers to directly compare satellite observations to laboratory- or field-measured spectra, reflectance data from other instruments, predictions of canopy radiative transfer models, or to measurements made by the same sensor over long times and/or large areas (Masek et al., 2006). By removing atmospheric noise to focus on the surface signal itself, surface reflectance datasets increase precision in mapping land-cover, surface water resources, vegetation biophysics, and land-cover changes (Masek et al., 2006; Townshend et al., 2012).

This expansive comparability is apparent in the global true-color mosaic of Landsat SR for the 2000 GLS epoch (Fig. 8) and over Cape Cod, Massachusetts, USA (longitude 72 W–67.5 W, latitude 41 N–46 N) (Fig. 9). Radiometric consistency is very high not only globally, but also among adjacent individual images, with greatly reduced need for histogram matching or other ad hoc techniques that are often employed to create visually consistent images.

Due to the reduction of atmospheric noise, surface features are also more clearly distinguishable in the SR than the TOA mosaic. Although some remnant atmospheric noise still contributes to differences between adjacent SR images, the effect of the atmosphere on image clarity is greatly diminished relative to TOA. Instead of haze or aerosol contamination, true land cover differences – including especially phenological variation of agricultural croplands and natural vegetation – are the dominant factors of heterogeneity in the data. Alongside ongoing improvements to corrections for atmospheric (e.g., cloud and aerosol), bidirectional (including terrain), and other effects, it appears that addressing phenological variation – either by image selection or model-based correction – is set to become the

next major advancement in systematic image processing for long-term land cover monitoring.

4.2. The first global Landsat SR product

Fig. 8 shows the first global, multi-temporal mapping of Earth's land surface by atmospheric correction of Landsat data. Masek et al. (2006) used an earlier version of the LEDAPS algorithm to produce seamless SR mosaics over North America, and Roy et al. (2010) used a novel temporal compositing approach to produce 30-meter terrain-corrected Landsat-7 ETM + mosaics at various temporal intervals over the conterminous United States (CONUS) and Alaska. But prior to this effort, atmospheric correction has not been applied consistently to Landsat data at the global scale, nor has such an extensive quality assessment been performed on any derived Landsat data product.

A large part of the success of this effort is due to the 6S atmospheric correction algorithm (Vermote et al., 1997b), whose foundation in physical radiative transfer theory yields benefits in both the short and long term. The LEDAPS implementation of 6S not only yields obvious immediate improvements to interpretation and analysis over of SR images over DN and TOA reflectance, but also provides a framework for advances in atmospheric science to be incorporated to improve data products over time. The globally applicable algorithm supports scalability of production and ensures spatial and temporal consistency of Landsat and Landsat-class data products, and the high level of consistency between Landsat and MODIS SR products will allow better integration of these two data types in many applications (e.g., Hilker et al., 2009; Potapov et al., 2008).

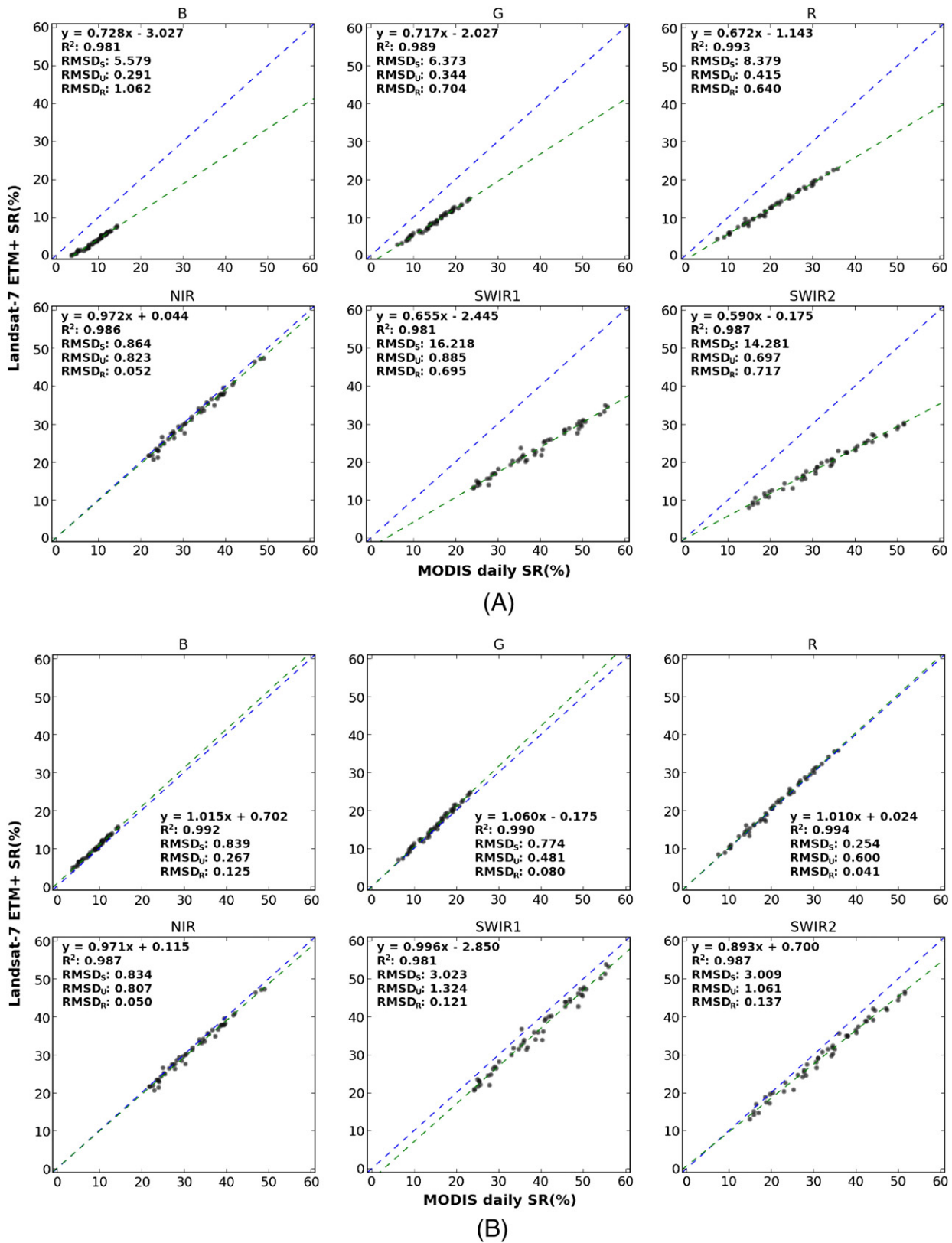


Fig. 6. Scatter plots for each band of the April 12, 2001 ETM+ image acquired over Morocco (WRS-2 path 200/row 37), based on H/L gain values (A) and LMIN/LMAX values (B) from the ETM+ metadata. The 1:1 (dashed blue line) and the linear regression line (dashed green line) are added to each chart.

To our knowledge, this effort has been the most systematic, consistent, and comprehensive comparison between global surface reflectance image datasets to date. Comparisons were performed at two

scales: globally in order to understand sources of error and at the scale of each Landsat image to provide image-level quality indicators, which are necessary to prevent problematic images from being used

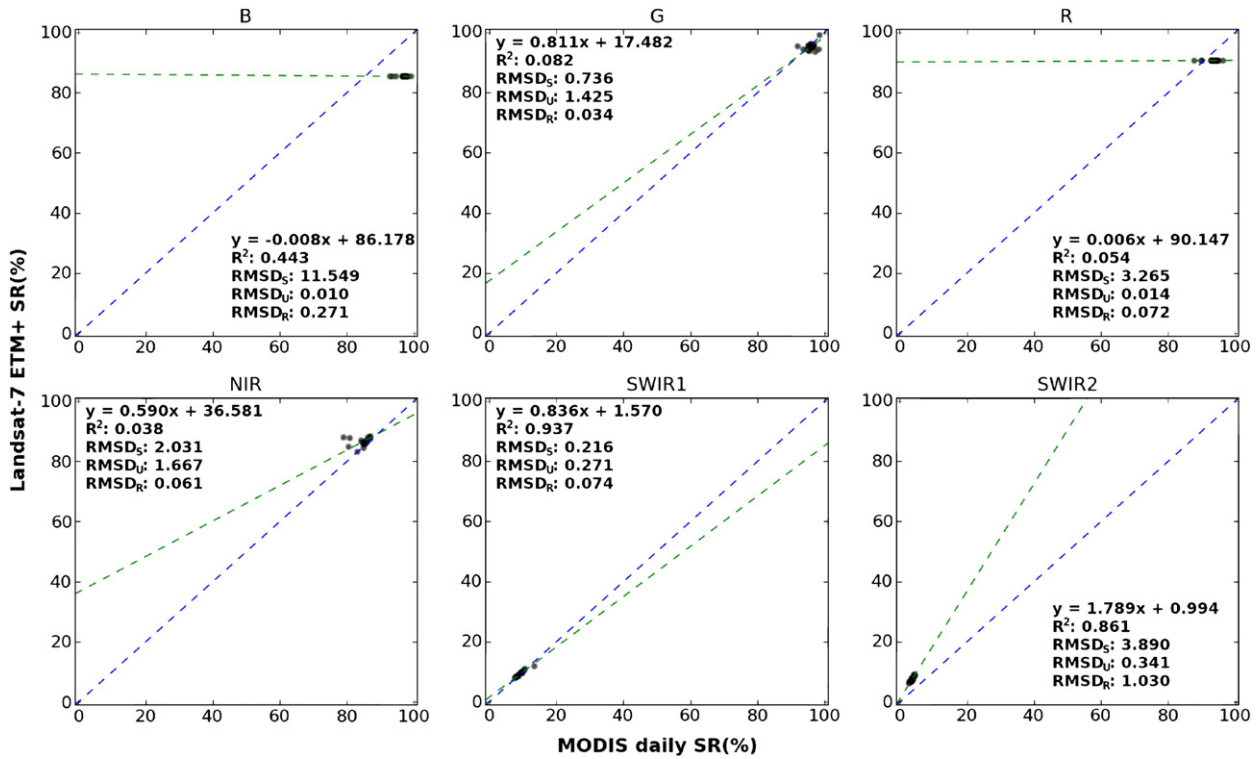


Fig. 7. Scatter plots for each band of the ETM + image acquired on June 5, 2001 over Greenland (WRS-2 path 9/row 5). The MODIS and Landsat values are represented at x-axis and y-axis respectively. The 1:1 (dashed blue line) and the linear regression line (dashed green line) are added to each chart.

in downstream applications. Whereas ground or in situ measurements are the preferred reference for assessing absolute errors in remotely sensed data products, reference data that are coincident with each image are also needed to detect image-specific errors resulting from incorrect ancillary data or metadata, or other sources (Feng et al., 2012). The global MODIS SR products, which are available from 2000-present, provide the best available data sources for testing Landsat-based SR products within the MODIS era. Our comparison with MODIS data was a relative assessment; however, given that MODIS SR products were derived and evaluated consistently at the global scale (Roy et al., 2002), have been rigorously evaluated using ground-based and other in situ observations (Liang et al., 2002; Vermote & Kotchenova, 2008a; Vermote et al., 2002), and were used

to derive other global data products that have themselves been assessed comprehensively (Friedl et al., 2002; Hansen et al., 2005; Myrneni et al., 2002; Roy et al., 2002; Running et al., 2004), a Landsat SR image consistent with MODIS data should be considered a reliable estimate of surface reflectance. The small differences between Landsat and MODIS SR values were mostly due to slightly different spectral responses of the two sensors and their calibration uncertainties. At the global scale, strong agreement between the Landsat ETM + and MODIS daily SR datasets suggests that overall quality of the Landsat SR products is high. Among-scene differences visible in the global Landsat SR mosaic (Fig. 8) were mostly due to actual differences in surface conditions arising from images acquired in different seasons and/or years (Kim et al., 2011; Townshend et al., 2012), although in extremely hazy areas

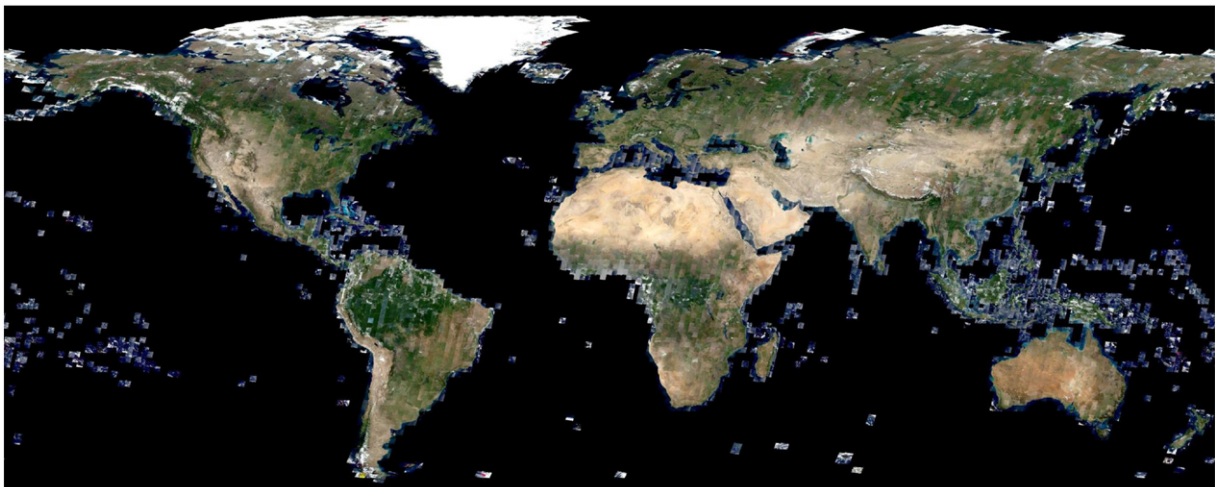


Fig. 8. Global, true-color (R, G, B) Landsat surface reflectance (SR) mosaic for the GLS 2000 epoch.

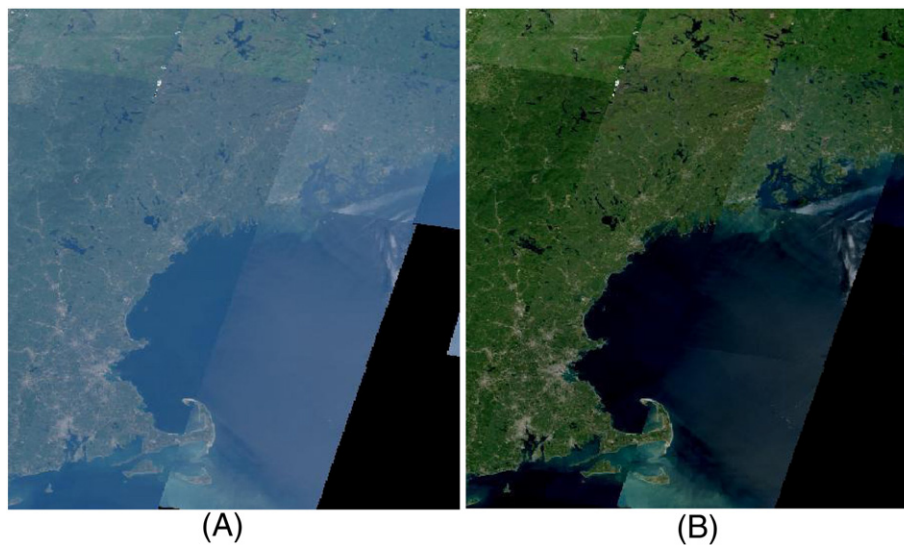


Fig. 9. Comparison between TOA (A) and SR (B) over Cape Cod, USA (longitude 72W–67.5W, latitude 41N–46N). Both SR and TOA mosaics are displayed with the same logarithmic stretch to ensure comparability (Appendix 3).

there could be residual atmospheric effects that could not be corrected by the LEDAPS algorithm. Strong agreement between Landsat-5 SR and MODIS NBAR suggest that similar quality can be expected for retrieval of SR from the Landsat archive prior to the MODIS era. Many Landsat-5 images from the Landsat archive – including those in the 1990 GLS epoch – do not currently have correct calibration parameters required to convert DN to radiance (Chander et al., 2009; Loveland & Dwyer, 2012), but USGS efforts to repatriate the raw (Level-0) data from international collaborators are ongoing. Only those TM images with the required radiometric information and coincident MODIS data are included in this analysis, but their assessment should be considered indicative of the quality of identically calibrated 1990 GLS images, as well as any other properly calibrated images from Landsat-5 or Landsat-7.

5. Conclusions

A global, multi-temporal surface reflectance dataset at Landsat (30-m) resolution has been produced by atmospheric correction of the GLS 2000 and 2005 datasets, followed by a comprehensive assessment of data quality relative to MODIS surface reflectance products. Consistency with MODIS daily SR and 16-day NBAR data is very high, with overall discrepancies between 1.3 and 2.8 percentage points for Landsat-7 ETM+ and between 2.2 and 3.5 percentage points for Landsat-5 TM. A comparison between the observed Landsat–MODIS differences and the measurement uncertainties of the two systems revealed that the observed Landsat–MODIS differences were within the two systems' measurement uncertainties in all bands but the SWIR1 band for the majority of the ETM+ images. This was also true for a smaller percentage of TM images, although the percentages were much lower for the infrared bands. Saturation of Landsat sensors over snow and ice, as well as cloud movement between MODIS and Landsat 7 overpass, were the likely reasons for most ETM+ images showing differences exceeding the measurement uncertainties of the two systems, and systematic biases between Landsat and MODIS SWIR bands were likely due to bandwidth differences between the two systems. Incorrect H/L gain settings as specified in the metadata file of some ETM+ images resulted in incorrect SR estimates, but this problem was corrected after the rescaling

gain/bias values were calculated using the LMIN and LMAX values provided in the same metadata files. In general, agreement between TM SR and MODIS NBAR data was also high, but agreement was not as high as was observed between ETM+ and MODIS daily SR data.

Because this assessment of Landsat SR was performed relative to MODIS estimates with similar model assumptions, there remains potential for shared errors between the two datasets. Assessment relative to a representative global sample of near-surface observations will be an important step for further research. Despite the ongoing need for refinement, routine production of Landsat-based surface reflectance data with strong correlation to MODIS retrievals is now possible. The 1990 epoch of the GLS will be processed following similar methods and added to the archive, followed by images selected to increase coverage of peak growing season and other conditions of interest. The dataset has been posted, along with a quality assessment report for each image, on the Global Land Cover Facility web site (http://www.landcover.org/data/gls_SR), where the images are available for free download. This first global surface reflectance dataset at sub-hectare resolution will serve as a valuable resource to the ecological, climatological, and other Earth science communities. As USGS is planning to make SR one of its standard imagery products for existing and future Landsat data, the Landsat–MODIS comparison approach tested globally through this study provides a mechanism for assessing each Landsat SR image, to the degree allowed by MODIS data availability. This approach can also be adapted for use in situations when MODIS data are not available but other global observations similar to MODIS data do exist. The ability to perform quality assessment of tens of thousands of Landsat SR images demonstrated in this study is unprecedented. Such a comprehensive assessment would essentially prevent erroneous imagery products from being distributed, and therefore greatly reduce users' burden in quality-screening of such products.

Acknowledgments

Funding support for this study was provided by the following NASA programs: Making Earth System Data Records for Use in Research Environments (NNH06ZDA001N-MEASURES), Land Cover and Land Use Change (NNH07ZDA001N-LCLUC), and Earth System Science Research Using Data and Products from Terra, Aqua, and

Acirmsat Satellites (NNH06ZDA001N-EOS). The MODIS daily products used in this study were obtained from Greg Ederer and Robert Wolfe (NASA Goddard Space Flight Center). The GLS datasets were sent to GLCF by Rachel Headley (USGS). We also acknowledge the three anonymous reviewers for their helpful comments on earlier versions of the manuscript.

Appendix 1. List of GLS Landsat images with erroneous radiometric gain values

GLS epoch	Sensor	WRS-2 path/row	Acquisition date
2000	Landsat-7 ETM +	p200r037	2001-04-12
2000	Landsat-7 ETM +	p031r001	2001-06-15
2000	Landsat-7 ETM +	p134r027	2001-08-20
2000	Landsat-7 ETM +	p004r014	2001-09-06
2000	Landsat-7 ETM +	p231r093	2001-01-15
2000	Landsat-7 ETM +	p175r012	2000-06-29
2000	Landsat-7 ETM +	p192r017	2001-05-06
2000	Landsat-7 ETM +	p176r036	2001-01-30
2000	Landsat-7 ETM +	p118r030	2001-09-21
2000	Landsat-7 ETM +	p133r019	2000-08-10
2000	Landsat-7 ETM +	p143r014	2001-07-18
2000	Landsat-7 ETM +	p134r039	2001-10-23
2000	Landsat-7 ETM +	p010r063	2000-10-31
2000	Landsat-7 ETM +	p097r013	2000-07-12
2000	Landsat-7 ETM +	p088r013	2000-07-13
2000	Landsat-7 ETM +	p035r001	2000-06-24
2000	Landsat-7 ETM +	p011r001	2000-07-02
2000	Landsat-7 ETM +	p099r016	2001-07-30
2000	Landsat-7 ETM +	p141r017	2001-08-05
2000	Landsat-7 ETM +	p168r014	2001-07-17
2000	Landsat-7 ETM +	p004r016	1999-07-31
2000	Landsat-7 ETM +	p102r017	2001-08-04
2000	Landsat-7 ETM +	p048r015	2001-07-24
2000	Landsat-7 ETM +	p186r038	2000-03-22
2000	Landsat-7 ETM +	p084r060	1999-06-29
2000	Landsat-7 ETM +	p114r031	2001-09-25
2000	Landsat-7 ETM +	p163r041	2000-04-22
2000	Landsat-7 ETM +	p085r050	2001-01-16
2000	Landsat-7 ETM +	p171r011	2000-06-01
2000	Landsat-7 ETM +	p070r015	2001-06-16
2000	Landsat-7 ETM +	p130r051	2000-12-27
2000	Landsat-7 ETM +	p161r027	2001-04-27
2000	Landsat-7 ETM +	p056r012	2000-06-11
2000	Landsat-7 ETM +	p099r024	2001-08-31
2000	Landsat-7 ETM +	p156r013	2001-07-13
2000	Landsat-7 ETM +	p197r033	2001-04-23
2000	Landsat-7 ETM +	p137r028	2001-06-06
2000	Landsat-7 ETM +	p021r013	2001-07-11
2000	Landsat-7 ETM +	p053r019	2001-08-12
2000	Landsat-7 ETM +	p179r012	2001-06-12
2000	Landsat-7 ETM +	p191r034	2001-02-08
2000	Landsat-7 ETM +	p165r007	2000-08-10
2000	Landsat-7 ETM +	p145r013	2001-07-16
2000	Landsat-7 ETM +	p132r036	2001-10-09
2000	Landsat-7 ETM +	p015r043	2001-11-06
2000	Landsat-7 ETM +	p148r029	2000-09-04
2000	Landsat-7 ETM +	p163r013	2000-07-11
2000	Landsat-7 ETM +	p173r037	2000-11-06
2000	Landsat-7 ETM +	p231r009	1999-07-05
2000	Landsat-7 ETM +	p151r032	2000-08-24
2000	Landsat-7 ETM +	p199r035	2002-04-24
2000	Landsat-7 ETM +	p109r018	2000-07-17
2000	Landsat-7 ETM +	p005r069	2001-06-25
2000	Landsat-7 ETM +	p033r001	2000-06-26
2000	Landsat-7 ETM +	p121r032	2000-09-07
2000	Landsat-7 ETM +	p152r032	2000-09-16
2000	Landsat-7 ETM +	p129r051	2002-01-08
2000	Landsat-7 ETM +	p136r039	2001-10-21
2000	Landsat-7 ETM +	p131r013	2000-07-11
2000	Landsat-7 ETM +	p067r015	2001-09-15
2000	Landsat-7 ETM +	p043r014	2000-07-18
2000	Landsat-7 ETM +	p163r026	2001-04-25
2000	Landsat-7 ETM +	p147r037	2000-10-15
2000	Landsat-7 ETM +	p103r016	2001-07-26

Appendix 1 (continued)

GLS epoch	Sensor	WRS-2 path/row	Acquisition date
2000	Landsat-7 ETM +	p022r001	2001-06-16
2000	Landsat-7 ETM +	p052r014	2000-07-17
2000	Landsat-7 ETM +	p143r025	2001-09-04
2000	Landsat-7 ETM +	p144r027	2000-08-07
2000	Landsat-7 ETM +	p105r018	2000-07-21
2000	Landsat-7 ETM +	p145r031	2000-05-10
2000	Landsat-7 ETM +	p023r012	2001-07-09
2000	Landsat-7 ETM +	p107r018	2001-06-20
2000	Landsat-7 ETM +	p206r041	2000-08-09
2000	Landsat-7 ETM +	p006r068	2001-08-03
2000	Landsat-7 ETM +	p039r015	2001-07-25
2000	Landsat-7 ETM +	p167r013	2000-07-07
2000	Landsat-7 ETM +	p178r006	2001-08-08
2000	Landsat-7 ETM +	p109r018	2001-09-22
2000	Landsat-7 ETM +	p127r051	2002-01-10
2000	Landsat-7 ETM +	p111r018	2000-07-15
2000	Landsat-7 ETM +	p174r012	2001-06-09
2000	Landsat-7 ETM +	p021r018	2000-08-09
2000	Landsat-7 ETM +	p014r041	2000-10-27
2000	Landsat-7 ETM +	p232r091	2001-12-08
2000	Landsat-7 ETM +	p193r035	2000-04-24
2000	Landsat-7 ETM +	p049r020	2001-08-16
2000	Landsat-7 ETM +	p179r007	2000-08-12
2000	Landsat-7 ETM +	p158r019	2001-08-12
2000	Landsat-7 ETM +	p218r013	2000-06-26
2000	Landsat-7 ETM +	p003r005	2000-06-08
2000	Landsat-7 ETM +	p034r013	2000-07-03
2000	Landsat-7 ETM +	p051r019	2001-08-14
2000	Landsat-7 ETM +	p139r035	2000-10-07
2000	Landsat-7 ETM +	p032r012	2001-07-08
2000	Landsat-7 ETM +	p176r038	2000-11-11
2000	Landsat-7 ETM +	p233r006	1999-07-03
2005	Landsat-7 ETM +	p176r011	2004-07-01
2005	Landsat-7 ETM +	p177r011	2004-07-08
2005	Landsat-7 ETM +	p172r043	2005-01-13

Appendix 2. List of GLS Landsat images affected by sensor saturation over snow-covered areas

GLS epoch	Sensor	WRS-2 path/row	Acquisition date
2000	Landsat-7 ETM +	p012r008	2001-07-28
2000	Landsat-7 ETM +	p230r013	2001-08-04
2000	Landsat-7 ETM +	p232r012	2001-08-02
2000	Landsat-7 ETM +	p019r004	2000-06-24
2000	Landsat-7 ETM +	p011r005	2000-07-02
2000	Landsat-7 ETM +	p004r013	2001-09-06
2000	Landsat-7 ETM +	p053r002	2002-07-30
2000	Landsat-7 ETM +	p219r015	2000-08-20
2000	Landsat-7 ETM +	p022r006	2001-07-18
2000	Landsat-7 ETM +	p054r022	2000-04-10
2000	Landsat-7 ETM +	p147r031	2000-09-13
2000	Landsat-7 ETM +	p233r013	2001-07-08
2000	Landsat-7 ETM +	p013r008	2001-06-01
2000	Landsat-7 ETM +	p006r015	2001-08-03
2000	Landsat-7 ETM +	p048r025	2000-09-23
2000	Landsat-7 ETM +	p233r009	2000-06-19
2000	Landsat-7 ETM +	p023r011	2001-07-09
2000	Landsat-7 ETM +	p049r025	2000-06-26
2000	Landsat-7 ETM +	p061r018	2001-07-19
2000	Landsat-7 ETM +	p003r004	2000-06-08
2000	Landsat-7 ETM +	p233r017	2001-07-08
2000	Landsat-7 ETM +	p233r018	2000-11-10
2000	Landsat-7 ETM +	p016r007	2001-06-06
2000	Landsat-7 ETM +	p033r002	2000-06-26
2000	Landsat-7 ETM +	p229r010	2001-07-12
2000	Landsat-7 ETM +	p009r010	2000-05-17
2000	Landsat-7 ETM +	p003r011	2000-06-08
2000	Landsat-7 ETM +	p011r004	2000-07-02
2000	Landsat-7 ETM +	p232r094	2001-05-14
2000	Landsat-7 ETM +	p023r011	2002-06-26
2000	Landsat-7 ETM +	p052r022	2000-05-30
2000	Landsat-7 ETM +	p232r093	2001-03-11

(continued on next page)

Appendix 2 (continued)

GLS epoch	Sensor	WRS-2 path/row	Acquisition date
2000	Landsat-7 ETM +	p048r003	2000-06-19
2000	Landsat-7 ETM +	p011r007	2000-07-02
2000	Landsat-7 ETM +	p006r012	2000-06-29
2000	Landsat-7 ETM +	p011r003	2000-07-02
2000	Landsat-7 ETM +	p009r009	2000-05-17
2000	Landsat-7 ETM +	p058r019	2001-08-15
2000	Landsat-7 ETM +	p015r008	2000-06-28
2000	Landsat-7 ETM +	p021r005	2000-07-24
2000	Landsat-7 ETM +	p025r003	2000-06-02
2000	Landsat-7 ETM +	p019r003	2000-06-24
2000	Landsat-7 ETM +	p026r005	2000-06-09
2000	Landsat-7 ETM +	p062r018	2001-06-08
2000	Landsat-7 ETM +	p009r009	2001-06-05
2000	Landsat-7 ETM +	p029r004	2000-06-14
2000	Landsat-7 ETM +	p012r008	2000-06-07
2000	Landsat-7 ETM +	p149r035	2000-10-29
2000	Landsat-7 ETM +	p004r014	2001-09-06
2000	Landsat-7 ETM +	p227r011	2000-08-28
2000	Landsat-7 ETM +	p006r014	2001-08-03
2000	Landsat-7 ETM +	p064r018	2001-09-10
2000	Landsat-7 ETM +	p006r006	2001-04-29
2000	Landsat-7 ETM +	p029r003	2000-06-14
2000	Landsat-7 ETM +	p013r010	2001-08-04
2000	Landsat-7 ETM +	p010r009	2000-09-13
2000	Landsat-7 ETM +	p232r013	2001-08-02
2000	Landsat-7 ETM +	p001r013	2001-06-13
2000	Landsat-7 ETM +	p009r003	2000-07-04
2000	Landsat-7 ETM +	p006r013	2001-08-03
2000	Landsat-7 ETM +	p233r014	2001-07-08
2000	Landsat-7 ETM +	p023r006	2001-08-26
2000	Landsat-7 ETM +	p031r005	2000-06-28
2000	Landsat-7 ETM +	p060r018	2001-08-13
2000	Landsat-7 ETM +	p037r007	2001-08-28
2000	Landsat-7 ETM +	p002r011	2001-06-04
2000	Landsat-7 ETM +	p056r001	2000-07-29
2000	Landsat-7 ETM +	p007r014	2001-07-09
2000	Landsat-7 ETM +	p004r012	2001-09-06
2000	Landsat-7 ETM +	p013r008	2001-08-04
2000	Landsat-7 ETM +	p016r002	2000-06-19
2000	Landsat-7 ETM +	p067r017	2002-08-01
2000	Landsat-7 ETM +	p219r014	2001-09-08
2000	Landsat-7 ETM +	p009r008	2001-06-05
2000	Landsat-7 ETM +	p062r017	2002-05-26
2000	Landsat-7 ETM +	p022r005	2002-06-19
2000	Landsat-7 ETM +	p012r009	2001-07-28
2000	Landsat-7 ETM +	p016r004	2000-06-19
2000	Landsat-7 ETM +	p009r007	2001-06-05
2000	Landsat-7 ETM +	p029r005	2000-06-14
2000	Landsat-7 ETM +	p231r007	2001-06-08
2000	Landsat-7 ETM +	p013r006	2001-06-01
2000	Landsat-7 ETM +	p139r035	2000-10-07
2000	Landsat-7 ETM +	p009r013	2001-07-07
2000	Landsat-7 ETM +	p040r005	2002-07-19
2000	Landsat-7 ETM +	p016r005	2000-06-19
2000	Landsat-7 ETM +	p035r001	2000-06-24
2000	Landsat-7 ETM +	p229r012	2001-07-12
2000	Landsat-7 ETM +	p003r010	2000-06-08
2000	Landsat-7 ETM +	p002r017	2000-08-04
2000	Landsat-7 ETM +	p050r024	2000-09-21
2000	Landsat-7 ETM +	p233r010	2000-06-19
2000	Landsat-7 ETM +	p003r007	2000-06-08
2000	Landsat-7 ETM +	p007r012	2001-07-09
2000	Landsat-7 ETM +	p019r006	2000-06-24
2000	Landsat-7 ETM +	p148r035	2001-05-18
2000	Landsat-7 ETM +	p064r017	2001-09-10
2000	Landsat-7 ETM +	p007r013	2001-07-09
2000	Landsat-7 ETM +	p016r005	2001-06-06
2000	Landsat-7 ETM +	p045r004	2000-06-14
2000	Landsat-7 ETM +	p057r020	2000-06-02
2000	Landsat-7 ETM +	p231r095	2001-10-14
2000	Landsat-7 ETM +	p056r012	2000-06-11
2000	Landsat-7 ETM +	p009r012	2001-07-07
2000	Landsat-7 ETM +	p002r008	2001-06-04
2000	Landsat-7 ETM +	p233r011	2000-06-19
2000	Landsat-7 ETM +	p231r094	2000-10-27
2000	Landsat-7 ETM +	p025r005	2000-06-02
2000	Landsat-7 ETM +	p021r004	2000-07-24

Appendix 2 (continued)

GLS epoch	Sensor	WRS-2 path/row	Acquisition date
2000	Landsat-7 ETM +	p025r001	2000-06-18
2000	Landsat-7 ETM +	p002r013	2001-06-04
2000	Landsat-7 ETM +	p029r002	2000-06-14
2000	Landsat-7 ETM +	p229r009	2001-07-12
2000	Landsat-7 ETM +	p008r010	2001-08-01
2000	Landsat-7 ETM +	p016r006	2001-06-06
2000	Landsat-7 ETM +	p069r018	2002-07-30
2000	Landsat-7 ETM +	p016r001	2000-06-19
2000	Landsat-7 ETM +	p004r015	2001-09-06
2000	Landsat-7 ETM +	p065r017	2002-08-03
2000	Landsat-7 ETM +	p021r006	2000-07-24
2000	Landsat-7 ETM +	p011r006	2000-07-02
2000	Landsat-7 ETM +	p178r006	2001-08-08
2000	Landsat-7 ETM +	p002r009	2001-06-04
2000	Landsat-7 ETM +	p010r010	2000-09-13
2000	Landsat-7 ETM +	p136r039	2001-10-21
2000	Landsat-7 ETM +	p013r009	2001-08-04
2000	Landsat-7 ETM +	p011r011	2000-07-02
2000	Landsat-7 ETM +	p021r002	2000-06-06
2000	Landsat-7 ETM +	p233r015	2001-07-08
2000	Landsat-7 ETM +	p001r012	2001-06-13
2000	Landsat-7 ETM +	p033r001	2000-06-26
2000	Landsat-7 ETM +	p019r005	2000-06-24
2000	Landsat-7 ETM +	p054r020	2002-03-15
2000	Landsat-7 ETM +	p011r006	2002-05-21
2000	Landsat-7 ETM +	p016r003	2000-06-19
2000	Landsat-7 ETM +	p009r011	2001-07-07
2000	Landsat-7 ETM +	p051r023	2000-06-24
2000	Landsat-7 ETM +	p003r006	2000-06-08
2000	Landsat-7 ETM +	p136r038	2001-10-21
2000	Landsat-7 ETM +	p013r007	2001-06-01
2000	Landsat-7 ETM +	p011r008	2000-07-02
2000	Landsat-7 ETM +	p025r004	2000-06-02
2000	Landsat-7 ETM +	p011r004	2002-06-06
2000	Landsat-7 ETM +	p006r013	2000-06-29
2000	Landsat-7 ETM +	p008r011	2001-08-01
2000	Landsat-7 ETM +	p006r011	2000-06-29
2000	Landsat-7 ETM +	p053r021	2001-08-12
2000	Landsat-7 ETM +	p003r005	2000-06-08
2000	Landsat-7 ETM +	p003r009	2000-06-08
2000	Landsat-7 ETM +	p227r010	2000-08-28
2000	Landsat-7 ETM +	p221r014	2000-09-19
2000	Landsat-7 ETM +	p229r011	2001-07-12
2000	Landsat-7 ETM +	p059r014	2002-05-21
2000	Landsat-7 ETM +	p021r003	2000-06-06
2000	Landsat-7 ETM +	p003r008	2000-06-08
2000	Landsat-7 ETM +	p233r016	2001-07-08
2000	Landsat-7 ETM +	p053r001	2002-07-30
2000	Landsat-7 ETM +	p054r008	2000-09-01
2000	Landsat-7 ETM +	p011r001	2000-07-02
2000	Landsat-7 ETM +	p075r022	2002-03-18
2000	Landsat-7 ETM +	p229r008	2001-07-12
2000	Landsat-7 ETM +	p060r004	2001-07-12
2000	Landsat-7 ETM +	p063r001	2002-06-18
2000	Landsat-7 ETM +	p227r009	2000-08-28
2000	Landsat-7 ETM +	p043r004	2000-06-16
2000	Landsat-7 ETM +	p230r014	2001-08-04
2000	Landsat-7 ETM +	p021r007	2000-07-24
2000	Landsat-7 ETM +	p228r008	2000-06-16
2000	Landsat-7 ETM +	p055r003	2000-06-20
2000	Landsat-7 ETM +	p040r006	2000-07-29
2000	Landsat-7 ETM +	p150r043	2001-09-21
2000	Landsat-7 ETM +	p039r006	2002-09-14
2000	Landsat-7 ETM +	p063r018	2000-08-31
2000	Landsat-7 ETM +	p005r003	2000-07-24
2000	Landsat-7 ETM +	p216r015	2000-09-16
2000	Landsat-7 ETM +	p060r005	2001-07-12
2000	Landsat-7 ETM +	p039r007	2002-09-14
2000	Landsat-7 ETM +	p046r001	2002-07-13
2000	Landsat-7 ETM +	p063r002	2002-06-18
2000	Landsat-7 ETM +	p037r006	2000-07-24
2000	Landsat-7 ETM +	p039r008	2002-09-14
2000	Landsat-7 ETM +	p027r005	2000-06-16
2000	Landsat-7 ETM +	p229r007	2001-07-12
2000	Landsat-7 ETM +	p038r005	2000-06-29
2000	Landsat-7 ETM +	p225r011	2001-08-01
2000	Landsat-7 ETM +	p015r009	2000-06-28

Appendix 2 (continued)

GLS epoch	Sensor	WRS-2 path/row	Acquisition date
2000	Landsat-7 ETM +	p065r018	2000-09-30
2000	Landsat-7 ETM +	p011r002	2000-07-02
2000	Landsat-7 ETM +	p227r012	2000-08-28
2000	Landsat-7 ETM +	p231r006	2001-06-08
2000	Landsat-7 ETM +	p232r095	2002-08-05
2000	Landsat-7 ETM +	p024r010	2002-08-20
2000	Landsat-7 ETM +	p174r006	2002-08-15
2000	Landsat-7 ETM +	p223r013	2000-09-01
2000	Landsat-7 ETM +	p031r005	2001-06-15
2000	Landsat-7 ETM +	p013r001	2001-07-03
2000	Landsat-7 ETM +	p026r006	2000-07-27
2000	Landsat-7 ETM +	p067r018	2002-09-02
2000	Landsat-7 ETM +	p011r010	2000-06-16
2000	Landsat-7 ETM +	p232r015	2001-08-02
2000	Landsat-7 ETM +	p032r011	2001-08-25
2000	Landsat-7 ETM +	p040r004	2000-06-27
2000	Landsat-7 ETM +	p057r005	2002-06-24
2000	Landsat-7 ETM +	p178r007	2001-08-08
2000	Landsat-7 ETM +	p228r012	2001-09-07
2000	Landsat-7 ETM +	p001r018	2000-06-26
2000	Landsat-7 ETM +	p012r007	2000-06-07
2000	Landsat-7 ETM +	p232r018	2000-06-28
2000	Landsat-7 ETM +	p233r018	2001-07-08
2000	Landsat-7 ETM +	p149r005	2000-07-09
2000	Landsat-7 ETM +	p075r021	2002-04-03
2000	Landsat-7 ETM +	p032r012	2002-06-25
2000	Landsat-7 ETM +	p022r007	2000-10-03
2000	Landsat-7 ETM +	p056r004	2001-06-14
2000	Landsat-7 ETM +	p161r042	2000-05-26
2000	Landsat-7 ETM +	p007r011	2001-07-09
2000	Landsat-7 ETM +	p021r001	2000-06-06
2000	Landsat-7 ETM +	p085r024	2000-06-22
2000	Landsat-7 ETM +	p002r010	2001-06-04
2000	Landsat-7 ETM +	p002r014	2001-06-04
2000	Landsat-7 ETM +	p064r003	2000-06-19
2000	Landsat-7 ETM +	p060r019	2001-08-13
2000	Landsat-7 ETM +	p078r023	2001-06-08
2000	Landsat-7 ETM +	p002r016	2000-08-04
2000	Landsat-7 ETM +	p002r012	2001-06-04
2000	Landsat-7 ETM +	p009r006	2001-06-05
2000	Landsat-7 ETM +	p081r075	2001-04-26
2000	Landsat-7 ETM +	p012r001	2000-06-07
2000	Landsat-7 ETM +	p055r016	2001-09-11
2000	Landsat-7 ETM +	p223r014	2000-06-13
2000	Landsat-7 ETM +	p009r005	2001-06-05
2000	Landsat-7 ETM +	p171r011	2000-06-01
2000	Landsat-7 ETM +	p218r016	2000-09-30
2000	Landsat-7 ETM +	p002r015	2001-06-04
2005	Landsat-7 ETM +	p120r015	2005-05-09
2005	Landsat-7 ETM +	p227r012	2005-07-25
2005	Landsat-7 ETM +	p219r013	2004-03-24
2005	Landsat-7 ETM +	p217r015	2006-07-22
2005	Landsat-7 ETM +	p011r011	2004-06-11
2005	Landsat-7 ETM +	p153r005	2006-07-06
2005	Landsat-7 ETM +	p006r014	2007-08-04
2005	Landsat-7 ETM +	p037r004	2007-08-13
2005	Landsat-7 ETM +	p231r094	2004-08-19
2005	Landsat-7 ETM +	p099r018	2007-05-28
2005	Landsat-7 ETM +	p025r005	2007-08-09
2005	Landsat-7 ETM +	p034r008	2006-09-22
2005	Landsat-7 ETM +	p228r012	2004-08-14
2005	Landsat-7 ETM +	p028r012	2005-04-18
2005	Landsat-7 ETM +	p041r001	2007-07-24
2005	Landsat-7 ETM +	p004r017	2007-07-21
2005	Landsat-7 ETM +	p198r012	2005-06-12
2005	Landsat-7 ETM +	p021r011	2007-09-14
2005	Landsat-7 ETM +	p009r014	2004-09-01
2005	Landsat-7 ETM +	p004r014	2007-09-23
2005	Landsat-7 ETM +	p198r013	2005-04-25
2005	Landsat-7 ETM +	p019r005	2007-08-15
2005	Landsat-7 ETM +	p015r015	2004-07-25
2005	Landsat-7 ETM +	p231r010	2005-07-21
2005	Landsat-7 ETM +	p197r010	2005-05-04
2005	Landsat-7 ETM +	p017r013	2005-07-10
2005	Landsat-7 ETM +	p199r015	2006-05-05
2005	Landsat-7 ETM +	p046r002	2007-06-09
2005	Landsat-7 ETM +	p010r020	2007-06-13

Appendix 2 (continued)

GLS epoch	Sensor	WRS-2 path/row	Acquisition date
2005	Landsat-7 ETM +	p147r006	2005-06-23
2005	Landsat-7 ETM +	p189r013	2005-04-26
2005	Landsat-7 ETM +	p046r012	2007-04-22
2005	Landsat-7 ETM +	p197r013	2006-05-07
2005	Landsat-7 ETM +	p022r002	2005-06-11
2005	Landsat-7 ETM +	p028r006	2007-08-14
2005	Landsat-7 ETM +	p021r003	2007-08-29
2005	Landsat-7 ETM +	p100r024	2007-06-04
2005	Landsat-7 ETM +	p011r006	2004-05-10
2005	Landsat-7 ETM +	p013r009	2006-09-19
2005	Landsat-7 ETM +	p032r008	2005-08-20
2005	Landsat-7 ETM +	p039r002	2007-07-26
2005	Landsat-7 ETM +	p190r015	2004-03-13
2005	Landsat-7 ETM +	p227r010	2005-07-25
2005	Landsat-7 ETM +	p179r006	2006-04-23
2005	Landsat-7 ETM +	p012r006	2007-09-15
2005	Landsat-7 ETM +	p021r004	2007-08-29
2005	Landsat-7 ETM +	p001r018	2007-10-20
2005	Landsat-7 ETM +	p163r028	2006-05-25
2005	Landsat-7 ETM +	p233r007	2005-07-19
2005	Landsat-7 ETM +	p009r009	2007-08-09
2005	Landsat-7 ETM +	p035r003	2005-07-08
2005	Landsat-7 ETM +	p227r011	2005-07-25
2005	Landsat-7 ETM +	p041r002	2007-08-09
2005	Landsat-7 ETM +	p012r001	2007-06-27
2005	Landsat-7 ETM +	p021r011	2005-06-04
2005	Landsat-7 ETM +	p026r006	2005-08-26
2005	Landsat-7 ETM +	p026r005	2007-09-17
2005	Landsat-7 ETM +	p147r035	2005-08-26
2005	Landsat-7 ETM +	p013r010	2006-09-19
2005	Landsat-7 ETM +	p021r001	2007-08-13
2005	Landsat-7 ETM +	p012r002	2005-07-23
2005	Landsat-7 ETM +	p022r002	2005-06-27
2005	Landsat-7 ETM +	p031r005	2007-08-19
2005	Landsat-7 ETM +	p177r020	2004-04-03
2005	Landsat-7 ETM +	p196r010	2005-06-14
2005	Landsat-7 ETM +	p015r014	2004-06-23
2005	Landsat-7 ETM +	p021r004	2007-08-13
2005	Landsat-7 ETM +	p016r008	2005-07-19
2005	Landsat-7 ETM +	p179r007	2004-07-06
2005	Landsat-7 ETM +	p022r006	2004-06-24
2005	Landsat-7 ETM +	p007r013	2005-08-05
2005	Landsat-7 ETM +	p002r014	2004-09-16
2005	Landsat-7 ETM +	p217r014	2005-09-21
2005	Landsat-7 ETM +	p035r005	2007-08-15
2005	Landsat-7 ETM +	p015r015	2004-07-09
2005	Landsat-7 ETM +	p037r003	2007-08-13
2005	Landsat-7 ETM +	p232r014	2005-08-29
2005	Landsat-7 ETM +	p051r001	2005-07-08
2005	Landsat-7 ETM +	p039r001	2007-08-11
2005	Landsat-7 ETM +	p030r006	2006-08-25
2005	Landsat-7 ETM +	p035r004	2005-06-22
2005	Landsat-7 ETM +	p008r011	2004-06-22
2005	Landsat-7 ETM +	p231r094	2005-02-27
2005	Landsat-7 ETM +	p027r005	2007-08-23
2005	Landsat-7 ETM +	p199r017	2004-05-31
2005	Landsat-7 ETM +	p012r001	2007-06-11
2005	Landsat-7 ETM +	p229r008	2007-08-14
2005	Landsat-7 ETM +	p021r001	2007-06-10
2005	Landsat-7 ETM +	p023r011	2005-09-06
2005	Landsat-7 ETM +	p021r007	2005-08-07
2005	Landsat-7 ETM +	p105r017	2006-06-04
2005	Landsat-7 ETM +	p198r014	2007-06-02
2005	Landsat-7 ETM +	p004r014	2007-10-09
2005	Landsat-7 ETM +	p012r009	2005-08-08
2005	Landsat-7 ETM +	p148r035	2004-08-14
2005	Landsat-7 ETM +	p041r002	2007-07-24
2005	Landsat-7 ETM +	p053r017	2005-03-16
2005	Landsat-7 ETM +	p146r006	2004-09-01
2005	Landsat-7 ETM +	p010r010	2006-07-28
2005	Landsat-7 ETM +	p219r014	2006-09-22
2005	Landsat-7 ETM +	p232r093	2005-04-23
2005	Landsat-7 ETM +	p219r015	2006-09-06
2005	Landsat-7 ETM +	p158r004	2005-07-06
2005	Landsat-7 ETM +	p231r008	2006-07-24
2005	Landsat-7 ETM +	p232r095	2006-02-21

(continued on next page)

Appendix 2 (continued)

GLS epoch	Sensor	WRS-2 path/row	Acquisition date
2005	Landsat-7 ETM +	p021r005	2007-08-29
2005	Landsat-7 ETM +	p003r005	2004-06-19
2005	Landsat-7 ETM +	p019r014	2004-03-31
2005	Landsat-7 ETM +	p009r011	2007-08-09
2005	Landsat-7 ETM +	p015r016	2006-09-17
2005	Landsat-7 ETM +	p231r095	2005-07-05
2005	Landsat-7 ETM +	p032r008	2007-07-09
2005	Landsat-7 ETM +	p009r014	2004-09-17
2005	Landsat-7 ETM +	p024r010	2006-07-14
2005	Landsat-7 ETM +	p149r035	2006-07-26
2005	Landsat-7 ETM +	p009r021	2005-04-29
2005	Landsat-7 ETM +	p017r016	2007-04-27
2005	Landsat-7 ETM +	p004r016	2007-07-21
2005	Landsat-7 ETM +	p009r012	2007-08-09
2005	Landsat-7 ETM +	p012r003	2006-07-26
2005	Landsat-7 ETM +	p233r013	2005-08-04
2005	Landsat-7 ETM +	p198r016	2005-04-25
2005	Landsat-7 ETM +	p019r012	2006-07-11
2005	Landsat-7 ETM +	p223r013	2005-07-13
2005	Landsat-7 ETM +	p074r018	2006-05-25
2005	Landsat-7 ETM +	p021r011	2007-07-12
2005	Landsat-7 ETM +	p016r004	2007-08-10
2005	Landsat-7 ETM +	p007r012	2007-08-11
2005	Landsat-7 ETM +	p019r002	2004-07-05
2005	Landsat-7 ETM +	p098r018	2006-10-25
2005	Landsat-7 ETM +	p015r009	2005-08-13
2005	Landsat-7 ETM +	p199r017	2005-03-31
2005	Landsat-7 ETM +	p007r023	2006-04-18
2005	Landsat-7 ETM +	p019r004	2007-08-31
2005	Landsat-7 ETM +	p046r002	2007-07-11
2005	Landsat-7 ETM +	p051r001	2005-06-22
2005	Landsat-7 ETM +	p232r011	2005-08-13
2005	Landsat-7 ETM +	p029r002	2007-08-21
2005	Landsat-7 ETM +	p231r009	2005-07-21
2005	Landsat-7 ETM +	p233r016	2004-08-17
2005	Landsat-7 ETM +	p231r096	2005-06-19
2005	Landsat-7 ETM +	p031r001	2007-07-18
2005	Landsat-7 ETM +	p031r004	2007-07-18
2005	Landsat-7 ETM +	p017r018	2005-03-20
2005	Landsat-7 ETM +	p034r008	2006-09-06
2005	Landsat-7 ETM +	p233r008	2005-07-19
2005	Landsat-7 ETM +	p230r012	2005-08-15
2005	Landsat-7 ETM +	p031r001	2007-06-16
2005	Landsat-7 ETM +	p151r035	2006-07-08
2005	Landsat-7 ETM +	p044r002	2005-06-05
2005	Landsat-7 ETM +	p233r006	2004-07-16
2005	Landsat-7 ETM +	p072r021	2004-11-13
2005	Landsat-7 ETM +	p217r015	2006-08-07
2005	Landsat-7 ETM +	p150r031	2006-05-14
2005	Landsat-7 ETM +	p026r005	2007-08-16
2005	Landsat-7 ETM +	p006r013	2007-08-04
2005	Landsat-7 ETM +	p232r015	2007-08-03
2005	Landsat-7 ETM +	p028r009	2006-07-10
2005	Landsat-7 ETM +	p005r003	2006-07-25
2005	Landsat-7 ETM +	p101r022	2006-05-23
2005	Landsat-7 ETM +	p015r013	2004-07-09
2005	Landsat-7 ETM +	p227r009	2007-09-01
2005	Landsat-7 ETM +	p032r008	2005-09-05
2005	Landsat-7 ETM +	p046r001	2005-07-05
2005	Landsat-7 ETM +	p019r004	2007-08-15
2005	Landsat-7 ETM +	p002r016	2004-09-16
2005	Landsat-7 ETM +	p154r007	2005-09-12
2005	Landsat-7 ETM +	p048r010	2006-06-04
2005	Landsat-7 ETM +	p030r009	2004-08-03
2005	Landsat-7 ETM +	p009r010	2007-08-25
2005	Landsat-7 ETM +	p154r007	2005-06-24
2005	Landsat-7 ETM +	p149r007	2004-09-22
2005	Landsat-7 ETM +	p007r011	2007-08-11
2005	Landsat-7 ETM +	p013r009	2006-08-02
2005	Landsat-7 ETM +	p011r011	2004-09-15
2005	Landsat-7 ETM +	p145r035	2006-10-18
2005	Landsat-7 ETM +	p007r014	2004-08-02
2005	Landsat-7 ETM +	p001r018	2007-10-04
2005	Landsat-7 ETM +	p008r014	2006-06-28
2005	Landsat-7 ETM +	p021r003	2007-08-13
2005	Landsat-7 ETM +	p019r005	2007-08-31
2005	Landsat-7 ETM +	p151r033	2005-08-22

Appendix 2 (continued)

GLS epoch	Sensor	WRS-2 path/row	Acquisition date
2005	Landsat-7 ETM +	p232r094	2006-02-21
2005	Landsat-7 ETM +	p007r011	2007-08-27
2005	Landsat-7 ETM +	p021r005	2007-08-13
2005	Landsat-7 ETM +	p072r021	2005-02-01
2005	Landsat-7 ETM +	p127r007	2007-06-17
2005	Landsat-7 ETM +	p100r023	2007-06-04
2005	Landsat-7 ETM +	p229r012	2005-08-24
2005	Landsat-7 ETM +	p010r021	2007-05-28
2005	Landsat-7 ETM +	p029r005	2007-08-21
2005	Landsat-7 ETM +	p232r094	2005-04-23
2005	Landsat-7 ETM +	p009r003	2004-07-15
2005	Landsat-7 ETM +	p147r036	2006-09-30
2005	Landsat-7 ETM +	p155r004	2005-07-01
2005	Landsat-7 ETM +	p220r014	2004-09-23
2005	Landsat-7 ETM +	p154r006	2005-06-24
2005	Landsat-7 ETM +	p028r006	2007-08-30
2005	Landsat-7 ETM +	p019r007	2006-09-13
2005	Landsat-7 ETM +	p229r009	2005-08-24
2005	Landsat-7 ETM +	p017r016	2005-10-14
2005	Landsat-7 ETM +	p232r013	2007-08-19
2005	Landsat-7 ETM +	p012r003	2005-06-21
2005	Landsat-7 ETM +	p009r006	2005-08-19
2005	Landsat-7 ETM +	p026r011	2005-07-09
2005	Landsat-7 ETM +	p002r017	2004-08-31
2005	Landsat-7 ETM +	p233r018	2004-08-01
2005	Landsat-7 ETM +	p006r015	2006-09-02
2005	Landsat-7 ETM +	p230r013	2005-08-31
2005	Landsat-7 ETM +	p148r031	2006-09-05
2005	Landsat-7 ETM +	p044r002	2005-06-21
2005	Landsat-7 ETM +	p006r012	2007-09-05
2005	Landsat-7 ETM +	p233r015	2004-07-16
2005	Landsat-7 ETM +	p233r009	2004-07-16
2005	Landsat-7 ETM +	p231r007	2007-08-12
2005	Landsat-7 ETM +	p197r012	2006-05-07
2005	Landsat-7 ETM +	p231r011	2007-09-13
2005	Landsat-7 ETM +	p012r006	2007-08-30
2005	Landsat-7 ETM +	p039r003	2007-08-11
2005	Landsat-7 ETM +	p029r002	2007-06-02

Appendix 3. Creation of the global Landsat SR mosaic

Global Landsat SR mosaics were created from the Landsat retrieved SR images in the Geographic Coordinate System (GCS) between 60N to 85S latitude and 180W to 180E longitude. To ensure manageable image sizes, the global mosaic maps were created with 0.02 degree resolution, with each map comprising 18,000 columns and 7250 rows. The Landsat pixels were reprojected from UTM to GCS and then aggregated from 30 m to 0.02° by averaging Landsat SR pixels within the coverage of each 0.02 degree size pixel. Landsat 3, 2, and 1 (R, G, B) bands were used to create true color maps. The reflectance values in each band were converted from percent reflectance to byte-size RGB color components using logarithmic equation:

$$c = 256 * (\log v - V_{\min}) / (V_{\max} - V_{\min})$$

where v is the percent reflectance scaled by 10,000, c is the byte color components, and V_{\min} and V_{\max} define the reflectance value range— $\log(150)$ and $\log(5000)$, respectively.

References

- Berterretche, M., Hudak, A. T., Cohen, W. B., Maierperger, T. K., Gower, S. T., & Dungan, J. (2005). Comparison of regression and geostatistical methods for mapping Leaf Area Index (LAI) with Landsat ETM+ data over a boreal forest. *Remote Sensing of Environment*, 96, 49–61. <http://dx.doi.org/10.1016/j.rse.2005.01.014>.
- Chander, G., Markham, B. L., & Helder, D. L. (2009). Summary of current radiometric calibration coefficients for Landsat MSS, TM, ETM+, and EO-1 ALI sensors. *Remote Sensing of Environment*, 113(5), 893–903. <http://dx.doi.org/10.1016/j.rse.2009.01.007>.
- Cohen, W. B., Maierperger, T. K., Gower, S. T., & Turner, D. P. (2003). An improved strategy for regression of biophysical variables and Landsat ETM+ data. *Remote Sensing of Environment*, 84, 561–571.

- Fang, H., Liang, S., Kim, H. Y., Townshend, J. R., Schaaf, C. L., Strahler, A. H., et al. (2007). Developing a spatially continuous 1 km surface albedo data set over North America from Terra MODIS products. *Journal of Geophysical Research*, 112(D20206), 0–20. <http://dx.doi.org/10.1029/2006JD008377>.
- Feng, M., Huang, C., Channan, S., Vermote, E. F., Masek, J. G., & Townshend, J. R. (2012). Quality assessment of Landsat surface reflectance products using MODIS data. *Computers & Geosciences*, 38(1), 9–22. <http://dx.doi.org/10.1016/j.cageo.2011.04.011>.
- Franks, S., Masek, J., Headley, R., Gasch, J., Covington, S., & Arvidson, T. (2009). Large Area Scene Selection Interface (LASSI): Methodology of Selecting Landsat Imagery for the Global Land Survey 2005. *Photogrammetric Engineering and Remote Sensing*, 75(11), 1287–1296.
- Friedl, M. A., Zhang, X. Y., Muchoney, D., Strahler, A. H., Woodcock, C. E., Gopal, S., et al. (2002). Global land cover mapping from MODIS: Algorithms and early results. *Remote Sensing of Environment*, 83, 287–302.
- Goward, S. N., & Williams, D. L. (1997). Landsat and Earth Systems Science: Development of terrestrial monitoring. *Photogrammetric Engineering and Remote Sensing*, 63(7), 887–900.
- Gutman, G., Byrnes, R., Masek, J., Covington, S., Justice, C., Franks, S., et al. (2008). Towards monitoring land-cover and land-use changes at a global scale: The Global Land Survey 2005. *Photogrammetric Engineering and Remote Sensing*, 74(1), 6–10.
- Hansen, M. C., Townshend, J. R. G., Defries, R. S., & Carroll, M. (2005). Estimation of tree cover using MODIS data at global, continental and regional/local scales. *International Journal of Remote Sensing*, 26, 4359–4380.
- Hilker, T., Wulder, M. A., Coops, N. C., Linke, J., McDermid, G., Masek, J. G., et al. (2009). A new data fusion model for high spatial- and temporal-resolution mapping of forest disturbance based on Landsat and MODIS. *Remote Sensing of Environment*, 113(8), 1613–1627. <http://dx.doi.org/10.1016/j.rse.2009.03.007>.
- Huang, C., Kim, S., Song, K., Townshend, J. R., Davis, P., Altstatt, A., et al. (2009). Assessment of Paraguay's forest cover change using Landsat observations. *Global and Planetary Change*, 67(1–2), 1–12. <http://dx.doi.org/10.1016/j.gloplacha.2008.12.009>.
- Huete, A., Didan, K., Miura, T., Rodriguez, E. P., Gao, X., & Ferreira, L. G. (2002). Overview of the radiometric and biophysical performance of the MODIS vegetation indices. *Remote Sensing of Environment*, 83(1–2), 195–213. [http://dx.doi.org/10.1016/S0034-4257\(02\)00096-2](http://dx.doi.org/10.1016/S0034-4257(02)00096-2).
- Ju, J., Roy, D. P., Vermote, E. F., Masek, J., & Kovalsky, V. (2012). Continental-scale validation of MODIS-based and LEDAPS Landsat ETM+ atmospheric correction methods. *Remote Sensing of Environment*, 122, 175–184. <http://dx.doi.org/10.1016/j.rse.2011.12.025>.
- Kangas, M., Heikinheimo, M., & Laine, V. (2001). Accuracy of NOAA AVHRR-based surface reflectance over a winter-time boreal surface – comparison with aircraft measurements and land-cover information. *Theoretical and Applied Climatology*, 70(1–4), 231–244. <http://dx.doi.org/10.1007/s007040170017>.
- Kaufman, Y. J., & Tanré, D. (1996). Strategy for direct and indirect methods for correcting the aerosol effect on remote sensing: From AVHRR to EOS–MODIS. *Remote Sensing of Environment*, 55(1), 65–79.
- Kim, D., Narashiman, R., Sexton, J. O., Huang, C., & Townshend, J. R. (2011). A methodology to select phenologically suitable Landsat scenes for forest change detection. *2011 IEEE International Geoscience and Remote Sensing Symposium (IGARSS)* (pp. 2613–2616). Landsat 7 Science Data Users Handbook (2009). *Landsat 7 Science Data users Handbook*. NASA Goddard Space Flight Center, Greenbelt Maryland: Landsat Project Science Office (<http://landsathandbook.gsfc.nasa.gov/handbook.html>).
- Liang, S., Fang, H., Chen, M., Shuey, C. J., Walthall, C., Daughtry, C., Morisette, J., Schaaf, C., & Strahler, A. (2002). Validating MODIS land surface reflectance and albedo products: Methods and preliminary results. *Remote Sensing of Environment*, 83, 149–162. [http://dx.doi.org/10.1016/S0034-4257\(02\)00092-5](http://dx.doi.org/10.1016/S0034-4257(02)00092-5).
- Lord, S. D. (1992). *A new software tool for computing earth's atmospheric transmission of near- and far-infrared radiation*. NASA Tech Memorandum 103957, Ames Research Center, Moffett Field, CA (http://ntrs.nasa.gov/archive/nasa/casi.ntrs.nasa.gov/19930010877_1993010877.pdf).
- Loveland, T. R., & Dwyer, J. L. (2012). Landsat: Building a strong future. *Remote Sensing of Environment*, 122, 22–29. <http://dx.doi.org/10.1016/j.rse.2011.09.022>.
- Markham, B. L., & Helder, D. L. (2012). Forty-year calibrated record of earth-reflected radiance from Landsat: A review. *Remote Sensing of Environment*, 122, 30–40. <http://dx.doi.org/10.1016/j.rse.2011.06.026>.
- Masek, J., Vermote, E., Saleous, N., Wolfe, R., Hall, F., Huemmerich, K., et al. (2006). A Landsat surface reflectance dataset for North America, 1990–2000. *IEEE Geoscience and Remote Sensing Letters*, 3(1), 68–72. <http://dx.doi.org/10.1109/LGRS.2005.857030>.
- Masuko, E., Wolfe, R., Sinno, S., & Teague, M. (2007). A disk-based system for producing and distributing science products from MODIS. *2007 IEEE International Geoscience and Remote Sensing Symposium* (pp. 3043–3046). <http://dx.doi.org/10.1109/IGARSS.2007.4423486>.
- Myneni, R. B., Hoffman, S., Knyazikhin, Y., Privette, J. L., Glassy, J., Tian, Y., et al. (2002). Global products of vegetation leaf area and fraction absorbed PAR from year one of MODIS data. *Remote Sensing of Environment*, 83, 214–231.
- Myneni, R. B., Nemani, R. R., & Running, S. W. (1997). Estimation of global leaf area index and absorbed par using radiative transfer models. *IEEE Geoscience and Remote Sensing*, 35(6), 1380–1393.
- Potapov, P., Hansen, M. C., Stehman, S. V., Loveland, T. R., & Pittman, K. (2008). Combining MODIS and Landsat imagery to estimate and map boreal forest cover loss. *Remote Sensing of Environment*, 112(9), 3708–3719. <http://dx.doi.org/10.1016/j.rse.2008.05.006>.
- Roy, D. P., Borak, J. S., Devadiga, S., Wolfe, R. E., Zheng, M., & Desloires, J. (2002). The MODIS Land product quality assessment approach. *Remote Sensing of Environment*, 83, 62.
- Roy, D. P., Ju, J., Kline, K., Scaramuzza, P. L., Kovalsky, V., Hansen, M., et al. (2010). Web-enabled Landsat Data (WELD): Landsat ETM+ composited mosaics of the conterminous United States. *Remote Sensing of Environment*, 114(1), 35–49. <http://dx.doi.org/10.1016/j.rse.2009.08.011>.
- Roy, D. P., Ju, J., Lewis, P., Schaaf, C., Gao, F., Hansen, M., et al. (2008). Multi-temporal MODIS–Landsat data fusion for relative radiometric normalization, gap filling, and prediction of Landsat data. *Remote Sensing of Environment*, 112, 3112–3130.
- Running, S. W., Nemani, R. R., Heinsch, F. A., Zhao, M., Reeves, M., & Hashimoto, H. (2004). A continuous satellite-derived measure of global terrestrial primary production. *BioScience*, 54, 547–560.
- Schaaf, C. B., Gao, F., Strahler, A. H., Lucht, W., Li, X., Tsang, T., et al. (2002). First operational BRDF, albedo NADIR reflectance products from MODIS. *Remote Sensing of Environment*, 83(1–2), 135–148. [http://dx.doi.org/10.1016/S0034-4257\(02\)00091-3](http://dx.doi.org/10.1016/S0034-4257(02)00091-3).
- Sexton, J. O., Urban, D. L., Donohue, M. J., & Song, C. (2013). Long-term land cover dynamics by multi-temporal classification across the Landsat-5 record. *Remote Sensing of Environment*, 128, 246–258.
- Sokal, R. R., & Rohlf, F. J. (1994). *Biometry: The principles and practices of statistics in biological research* (3rd ed.). San Francisco, CA: W. H. Freeman.
- Song, C., Woodcock, C. E., Seto, K. C., Lenney, M. P., & Macomber, S. A. (2001). Classification and change detection using Landsat TM data when and how to correct atmospheric effects? *Remote Sensing of Environment*, 75(2), 230–244. [http://dx.doi.org/10.1016/S0034-4257\(00\)00169-3](http://dx.doi.org/10.1016/S0034-4257(00)00169-3).
- Stevens, S. S. (1946). On the theory of scales of measurement. *Science*, 103(2684), 677–680.
- Townshend, J. R., Justice, C., Li, W., Gurney, C., & Mcmanus, J. (1991). Global land cover classification by remote sensing: Present capabilities and future possibilities. *Remote Sensing of Environment*, 35(2–3), 243–255. [http://dx.doi.org/10.1016/0034-4257\(91\)90016-Y](http://dx.doi.org/10.1016/0034-4257(91)90016-Y).
- Townshend, J. R., Masek, J. G., Huang, C. Q., Vermote, E. F., Gao, F., Channan, S., et al. (2012). Global characterization and monitoring of forest cover using Landsat data: Opportunities and challenges. *International Journal of Digital Earth*, 5, 373–397. <http://dx.doi.org/10.1080/17538947.2012.713190>.
- Tucker, C. J., Grant, D. M., & Dykstra, J. D. (2004). NASA's global orthorectified Landsat data set. *Photogrammetric Engineering and Remote Sensing*, 70(3), 313–322.
- Vermote, E. F., El Saleous, N., Justice, C. O., Kaufman, Y. J., Privette, J. L., Remer, L., et al. (1997). Atmospheric correction of visible to middle-infrared EOS–MODIS data over land surfaces: Background, operational algorithm and validation. *Journal of Geophysical Research*, 102(D14), 17131–17141. <http://dx.doi.org/10.1029/97JD00201>.
- Vermote, E. F., & Kotchenova, S. Y. (2008a). MOD09 (Surface Reflectance) User's Guide. Available at: http://modis-sr.ltdri.org/products/MOD09_UserGuide_v1_2.pdf
- Vermote, E. F., & Kotchenova, S. Y. (2008b). Atmospheric correction for the monitoring of land surfaces. *Journal of Geophysical Research*, 113(D23), D23590. <http://dx.doi.org/10.1029/2007JD009662>.
- Vermote, E. F., & Saleous, N. Z. (2006). Operational atmospheric correction of MODIS visible to middle infrared land surface data in the case of an infinite Lambertian target. In J. Q. Qu, W. Gao, M. Kafatos, R. E. Murphy, & V. V. Salomonson (Eds.), *Earth science satellite remote sensing. Science and Instruments, Vol.1*. (pp. 123–153). Beijing: Tsinghua University Press.
- Vermote, E. F., Saleous, N. Z., & Justice, C. O. (2002). Atmospheric correction of MODIS data in the visible to middle infrared: First results. *Remote Sensing of Environment*, 83(1–2), 97–111. [http://dx.doi.org/10.1016/S0034-4257\(02\)00089-5](http://dx.doi.org/10.1016/S0034-4257(02)00089-5).
- Vermote, E. F., Saleous, N. Z., & Privette, J. L. (2006). *Surface reflectance earth system data record/climate data record white paper*. Greenbelt, MD: NASA, 6.
- Vermote, E. F., Tanre, D., Deuze, J. L., Herman, M., & Morcrette, J. J. (1997). Second simulation of the satellite signal in the solar spectrum, 6S: An overview. *IEEE Transactions on Geoscience and Remote Sensing*, 35(3), 675–686. <http://dx.doi.org/10.1109/36.581987>.
- Wang, Y., Lyapustin, A. I., Privette, J. L., Morisette, J. T., & Holben, B. (2009). Atmospheric correction at AERONET locations: A new science and validation data set. *IEEE Transactions on Geoscience and Remote Sensing*, 47, 2450–2466. <http://dx.doi.org/10.1109/TGRS.2009.2016334>.
- Willmott, C. J. (1982). Some comments on the evaluation of model performance. *Bulletin of the American Meteorological Society*, 63(11), 1309–1313.
- Xiong, X., Sun, J., Barnes, W., Salomonson, V., Esposito, J., Erives, H., et al. (2007). Multiyear on-orbit calibration and performance of Terra MODIS reflective solar bands. *IEEE Transactions on Geoscience and Remote Sensing*, 45(4), 879–889. <http://dx.doi.org/10.1109/TGRS.2006.890567>.
- Yamaguchi, Y., Kahle, A., Tsu, H., Kawakami, T., & Pniel, M. (1998). Overview of Advanced Spaceborne Thermal Emission and Reflection Radiometer (ASTER). *IEEE Transactions on Geoscience and Remote Sensing*, 36(4), 1062–1071. <http://dx.doi.org/10.1109/36.700991>.